



# **NAVAL POSTGRADUATE SCHOOL**

**MONTEREY, CALIFORNIA**

## **THESIS**

**BEAM CONTROL OF EXTREMELY AGILE RELAYING  
LASER SOURCE FOR BIFOCAL RELAY MIRROR  
SPACECRAFT**

by

Scott L. Johnson

September 2006

Thesis Advisor:  
Second Reader:

Brij Agrawal  
Jae Jun Kim

**Approved for public release, distribution is unlimited**

THIS PAGE INTENTIONALLY LEFT BLANK

<b>REPORT DOCUMENTATION PAGE</b>			<i>Form Approved OMB No. 0704-0188</i>	
Public reporting burden for this collection of information is estimated to average 1 hour per response, including the time for reviewing instruction, searching existing data sources, gathering and maintaining the data needed, and completing and reviewing the collection of information. Send comments regarding this burden estimate or any other aspect of this collection of information, including suggestions for reducing this burden, to Washington headquarters Services, Directorate for Information Operations and Reports, 1215 Jefferson Davis Highway, Suite 1204, Arlington, VA 22202-4302, and to the Office of Management and Budget, Paperwork Reduction Project (0704-0188) Washington DC 20503.				
<b>1. AGENCY USE ONLY (Leave blank)</b>		<b>2. REPORT DATE</b> September 2006	<b>3. REPORT TYPE AND DATES COVERED</b> Master's Thesis	
<b>4. TITLE AND SUBTITLE:</b> Beam Control of Extremely Agile Relaying Laser Source for Bifocal Relay Mirror Spacecraft			<b>5. FUNDING NUMBERS</b>	
<b>6. AUTHOR(S)</b> Scott L. Johnson				
<b>7. PERFORMING ORGANIZATION NAME(S) AND ADDRESS(ES)</b> Naval Postgraduate School Monterey, CA 93943-5000			<b>8. PERFORMING ORGANIZATION REPORT NUMBER</b>	
<b>9. SPONSORING / MONITORING AGENCY NAME(S) AND ADDRESS(ES)</b> N/A			<b>10. SPONSORING/MONITORING AGENCY REPORT NUMBER</b>	
<b>11. SUPPLEMENTARY NOTES</b> The views expressed in this thesis are those of the author and do not reflect the official policy or position of the Department of Defense or the U.S. Government.				
<b>12a. DISTRIBUTION / AVAILABILITY STATEMENT</b> Approved for public release; distribution is unlimited			<b>12b. DISTRIBUTION CODE</b>	
<b>13. ABSTRACT (maximum 200 words)</b> The concept of controlling optical laser beams on spacecraft for acquisition, tracking and pointing purposes is quickly becoming a reality. As a result, fine pointing of laser beams is turn out to be an increasingly important research topic. A unique testbed was constructed in order to study and develop new methods for laser beam control. This testbed, the Moving Target-Source Test Fixture (MTSTF), hosts a laser source, the Extremely Agile Relaying Laser Source (EARLS), which has the capability of automatically acquiring and directing a laser beam onto a satellite simulator while in motion. The purpose of this thesis is to make the EARLS platform operational by developing a tracking control system. The ultimate goal is to point the laser beam at the satellite simulator's receiving telescope and maintain the laser within the telescope's limits in the presence of structural disturbance induced by the EARLS motion.				
<b>14. SUBJECT TERMS</b> Adaptive Optics and Motor Manipulation, Beam Control			<b>15. NUMBER OF PAGES</b> 109	
			<b>16. PRICE CODE</b>	
<b>17. SECURITY CLASSIFICATION OF REPORT</b> Unclassified	<b>18. SECURITY CLASSIFICATION OF THIS PAGE</b> Unclassified	<b>19. SECURITY CLASSIFICATION OF ABSTRACT</b> Unclassified	<b>20. LIMITATION OF ABSTRACT</b> UL	

NSN 7540-01-280-5500

Standard Form 298 (Rev. 2-89)  
Prescribed by ANSI Std. Z39-18

THIS PAGE INTENTIONALLY LEFT BLANK

**Approved for public release; distribution is unlimited**

**BEAM CONTROL OF EXTREMELY AGILE RELAYING LASER SOURCE  
FOR BIFOCAL RELAY MIRROR SPACECRAFT**

Scott L. Johnson  
Lieutenant Commander, United States Coast Guard  
B.S., Norwich University, 1994

Submitted in partial fulfillment of the  
requirements for the degree of

**MASTER OF SCIENCE IN MECHANICAL ENGINEERING**

from the

**NAVAL POSTGRADUATE SCHOOL  
September 2006**

Author: Scott L. Johnson

Approved by: Brij Agrawal  
Thesis Advisor

Jae Jun Kim  
Second Reader

Anthony Healey  
Chairman, Department of Mechanical and Astronautical  
Engineering

THIS PAGE INTENTIONALLY LEFT BLANK

## **ABSTRACT**

The concept of controlling optical laser beams on spacecraft for acquisition, tracking and pointing purposes is quickly becoming a reality. As a result, fine pointing of laser beams is turn out to be an increasingly important research topic. A unique testbed was constructed in order to study and develop new methods for laser beam control. This testbed, the Moving Target-Source Test Fixture (MTSTF), hosts a laser source, the Extremely Agile Relaying Laser Source (EARLS), which has the capability of automatically acquiring and directing a laser beam onto a satellite simulator while in motion. The purpose of this thesis is to make the EARLS platform operational by developing a tracking control system. The ultimate goal is to point the laser beam at the satellite simulator's receiving telescope and maintain the laser within the telescope's limits in the presence of structural disturbance induced by the EARLS motion.

THIS PAGE INTENTIONALLY LEFT BLANK



# TABLE OF CONTENTS

<b>I.</b>	<b>INTRODUCTION.....</b>	<b>1</b>
<b>A.</b>	<b>BACKGROUND .....</b>	<b>1</b>
1.	Motivation.....	1
2.	Historical Context .....	1
3.	Bifocal Relay Mirror Laboratory.....	3
<b>B.</b>	<b>Thesis Overview .....</b>	<b>5</b>
<b>II.</b>	<b>EXPERIMENTAL SETUP .....</b>	<b>7</b>
<b>A.</b>	<b>THREE AXIS SATELLITE SIMULATOR TESTBED (TASS) .....</b>	<b>7</b>
<b>B.</b>	<b>MOVING TARGET-SOURCE TEST FIXTURE (MTSTF).....</b>	<b>9</b>
1.	Moving Target-Source Fixture Drive Components .....	10
a.	<i>Linear Track</i> .....	10
b.	<i>Prime Movers</i> .....	12
c.	<i>Controller</i> .....	12
2.	Extremely Agile Relaying Laser Source (EARLS) .....	12
a.	<i>Fast Steering Mirror (FSM)</i> .....	14
b.	<i>Video Camera</i> .....	15
c.	<i>Laser Assembly Platform</i> .....	16
<b>III.</b>	<b>SYSTEM IDENTIFICATION.....</b>	<b>17</b>
<b>A.</b>	<b>OVERVIEW.....</b>	<b>17</b>
<b>B.</b>	<b>TRANSFER FUNCTION OF AZIMUTH AND ELEVATION MOTORS.....</b>	<b>17</b>
1.	Mathematical Approach to Determining the Transfer Function ..	17
2.	Determination of Motor Transfer Functions .....	21
<b>C.</b>	<b>TRANSFER FUNCTION OF FAST STEERING MIRROR .....</b>	<b>25</b>
1.	Transfer Function for X Tip-Tilt Direction.....	26
2.	Transfer Function for Y Tip-Tilt Direction.....	29
<b>IV.</b>	<b>CONTROL METHODS.....</b>	<b>33</b>
<b>A.</b>	<b>OVERVIEW.....</b>	<b>33</b>
<b>B.</b>	<b>FAST STEERING MIRROR CONTROL .....</b>	<b>33</b>
1.	Input Shaping Theory.....	33
<b>C.</b>	<b>MOTOR CONTROL.....</b>	<b>42</b>
<b>V.</b>	<b>CONTROL ALGORITHM PROGRESSION .....</b>	<b>43</b>
<b>A.</b>	<b>OVERVIEW.....</b>	<b>43</b>
<b>B.</b>	<b>CALIBRATION SEQUENCE .....</b>	<b>43</b>
<b>C.</b>	<b>BEACON LOCATING SEQUENCE.....</b>	<b>46</b>
<b>D.</b>	<b>CONTROL SEQUENCE .....</b>	<b>46</b>
<b>VI.</b>	<b>RESULTS AND ANALYSIS .....</b>	<b>47</b>
<b>A.</b>	<b>OVERALL RESULTS.....</b>	<b>47</b>
<b>B.</b>	<b>SYSTEM PERFORMANCE IN THE X-DIRECTION .....</b>	<b>49</b>
<b>C.</b>	<b>SYSTEM PERFORMANCE IN THE Y-DIRECTION .....</b>	<b>51</b>

<b>VII</b>	<b>CONCLUSIONS AND RECOMMENDATIONS.....</b>	<b>55</b>
<b>A.</b>	<b>CONCLUSION .....</b>	<b>55</b>
<b>B.</b>	<b>FUTURE WORK.....</b>	<b>55</b>
<b>APPENDIX A:</b>	<b>LINEAR TRACK DATA .....</b>	<b>57</b>
<b>APPENDIX B:</b>	<b>PRIME MOVER DATA.....</b>	<b>59</b>
<b>APPENDIX C:</b>	<b>CONTROLLER DATA.....</b>	<b>61</b>
<b>APPENDIX D:</b>	<b>VIDEO CAMERA DATA .....</b>	<b>63</b>
<b>APPENDIX E:</b>	<b>MOTOR TRANSFER FUNCTION DATA.....</b>	<b>65</b>
<b>APPENDIX F:</b>	<b>MATLAB CODE FOR DETERMINING THE MOTOR TRANSFER FUNCTIONS .....</b>	<b>67</b>
<b>APPENDIX G:</b>	<b>MATLAB CODE FOR FSM EXPERIMENTAL TESTING .....</b>	<b>77</b>
<b>APPENDIX H:</b>	<b>SIMULINK MODEL OF FAST STEERING MIRROR .....</b>	<b>79</b>
<b>APPENDIX I:</b>	<b>MATLAB CODE FOR MOTOR AND FAST STEERING MIRROR CONTROL .....</b>	<b>81</b>
	<b>LIST OF REFERENCES.....</b>	<b>91</b>
	<b>INITIAL DISTRIBUTION LIST .....</b>	<b>93</b>

## LIST OF FIGURES

Figure 1.	Relay Mirror Experiment [From Chernesky, 2001] .....	2
Figure 2.	Bifocal Relay Mirror Spacecraft.....	3
Figure 3.	Bifocal Relay Mirror Operational Concept.....	4
Figure 4.	Three Axis Satellite Simulator #2 (TASS2) .....	7
Figure 5.	TASS2 Optical Payload .....	8
Figure 6.	Moving Target-Source Test Fixture (MTSTF) .....	9
Figure 7.	Experimental Layout.....	10
Figure 8.	MTSF Highlighting Independently Operated Linear Actuators .....	11
Figure 9.	Extremely Agile Relaying Laser Source (EARLS) .....	13
Figure 10.	Fast Steering Mirror (FSM) .....	14
Figure 11.	Location of LED Beacons on TASS2.....	15
Figure 12.	Electrical Schematic of a DC Motor .....	17
Figure 13.	General Motor Model .....	20
Figure 14.	Elevation Motor Velocity Measurements - Up Direction.....	22
Figure 15.	Elevation Motor Velocity Measurements - Down Direction.....	23
Figure 16.	Azimuth Motor Velocity Measurements - Back Direction.....	23
Figure 17.	Azimuth Motor Velocity Measurements - Forward Direction .....	24
Figure 18.	Fast Steering Mirror Experimental Testing Set Up .....	25
Figure 19.	Frequency Response of Fast Steering Mirror in X-Direction.....	26
Figure 20.	Bode Plot of Experimental Data for X Direction.....	27
Figure 21.	Bode Plot of Transfer Function for X direction.....	28
Figure 22.	Frequency Response of Fast Steering Mirror in Y-Direction.....	29
Figure 23.	Bode Plot of Experimental Data for Y Direction.....	30
Figure 24.	Bode Plot of Transfer Function for Y direction.....	31
Figure 25.	Two Impulse Response [From Sing, Singhouse].....	34
Figure 26.	Continuous Shaped Input [Sing, Singhouse] .....	37
Figure 27.	Shaped Input for X-direction .....	38
Figure 28.	Fast Steering Mirror Response For X-Direction.....	39
Figure 29.	Shaped Input for Y-direction .....	40
Figure 30.	Fast Steering Mirror Response For Y-Direction.....	41
Figure 31.	Cartoon of Camera Image of LEDs .....	44
Figure 32.	Cartoon of Camera Image of LEDs with Telescope Location.....	44
Figure 33.	Cartoon of Rotated Camera Image of LEDs with Telescope Location .....	45
Figure 34.	X-Direction Actual Error .....	48
Figure 35.	Y-Direction Actual Error .....	49
Figure 36.	Azimuth Motor and Fast Steering Mirror Voltages for the X-direction.....	50
Figure 37.	Comparison Between Error and Mirror Movement in the X-direction .....	51
Figure 38.	Comparison Between Error and Mirror Movement in the Y-direction .....	52
Figure 39.	Elevation Motor and Fast Steering Mirror Voltages for the Y-direction.....	53

THIS PAGE INTENTIONALLY LEFT BLANK

## LIST OF TABLES

Table 1.	Motor Transfer Functions .....	21
Table 2.	Input Shaping Values for Fast Steering Mirror.....	38

THIS PAGE INTENTIONALLY LEFT BLANK

## **ACKNOWLEDGMENTS**

I would like to express my sincere appreciation to Dr Brij Agrawal for allowing me to join his design team and utilize his laboratories for my thesis research. I'm especially grateful for his unparalleled support ensuring that I had all the available tools necessary to complete my thesis. I believe that my academic experience at NPS was much more fulfilling and meaningful as a result of my involvement with his team.

I would like to give special thanks to Dr. Jae Jun Kim for providing me with invaluable coaching and guidance throughout my thesis process. Dr. Kim imparted an overabundance of engineering knowledge onto me especially when it came to transforming theory I learned in the classroom into practical application. His personal attention kept me on track and more importantly instilled the confidence I needed to bring my thesis to fruition. Thanks Jae!

I would like to thank Major Tim Sands, USAF for recruiting me to the SRDC team. It was a great fit. I appreciate the hours of explaining difficult controls concepts to me in "layman's terms."

Lastly, I would like to thank Michael Doherty for his support. Mike was always "Johnny on the spot" when I had a technical issue. Also, his timely work on the MTSTF testbed was key to my success. Thanks Mike.

THIS PAGE INTENTIONALLY LEFT BLANK



# **I. INTRODUCTION**

## **A. BACKGROUND**

### **1. Motivation**

The recent advancements in laser technology have made possible the concept of using lasers on spacecraft for targeting ground-based objects. Lasers on spacecraft can be used for communications, target acquisition as well as imaging. While this concept is a possibility it does present several challenging engineering problems that must be overcome prior to full scale testing. In particular, the greatest challenge is fine pointing of a laser beam in the presence of structural vibrations.

All spacecraft has machinery that rotates and hence produce vibrations throughout the structure. While this vibration may be small it has an exaggerated effect on laser beam pointing. The undesired movement in the laser beam is termed “jitter.” As Watkins states in his PhD dissertation[Watkins, 2004], “A 100mm diameter laser beam with 10  $\mu$ rad of jitter will result in roughly a 400 fold decrease in the intensity of the beam at 100 km, due to jitter alone.” Jitter can also be induced by maneuvering the spacecraft with thrusters and exciting natural frequencies. This is particularly problematic since a typical spacecraft has very little structural damping so vibrations can take several minutes to diminish.

In order to study these problems and produce solutions the Naval Postgraduate School created the Bifocal Relay Mirror Laboratory (BFRM). This laboratory has testbeds that simulate the spacecraft and laser system in space like conditions. This thesis focuses on the development of a tracking control system for a laser source system in the BFRM Laboratory while reducing being subject to structural disturbances.

### **2. Historical Context**

The BFRM Spacecraft Project has its roots in Strategic Defense Initiative (SDI) experiments during the late 1980’s and early 1990’s. Specifically, the Relay Mirror

Experiment (RME) which successfully targeted a ground based laser on an orbiting satellite then reflected the laser radiation to another ground facility.

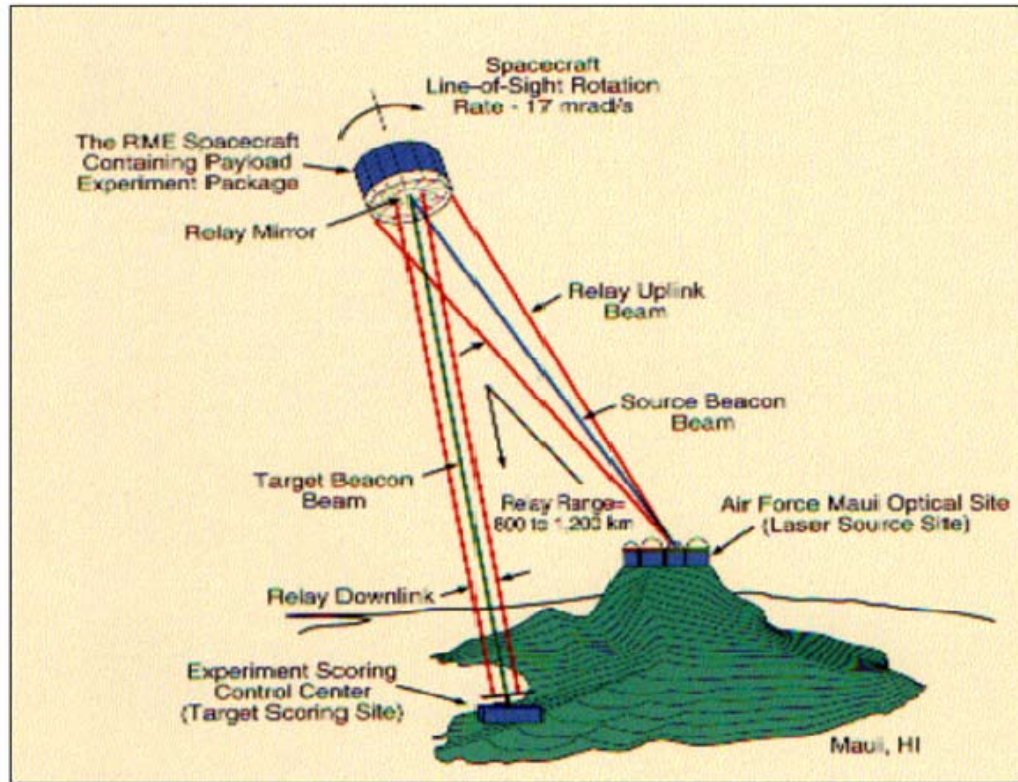


**Figure 1. Relay Mirror Experiment [From Chernesky, 2001]**

The motivation behind this experiment was its potential application to ballistic missile defense. Shortly afterwards public policy changed and the motivation to continue with the experiment was lost. However, the United States Air Force continued working on some of the technical challenges posed by the Relay Mirror Experiment for its airborne laser system such as laser beam forming, beam tracking and pointing and jitter control. In the late 1990's a study performed by the Air Force Research Laboratory recognized potential missions for a space based optical relay mirror. Among these missions are camouflage detection and penetration, chemical warfare agent detection and identification, illumination for nighttime operation and active imaging, and a laser fence for aircraft detection and underground structure detection.

### 3. Bifocal Relay Mirror Laboratory

In 2000, a preliminary satellite design was completed by a team of Naval Postgraduate School masters students resulting in a scissor-like Bifocal Relay Mirror spacecraft. The spacecraft consists of two optically coupled telescopes including adaptive optics used to redirect the light from a ground based laser to a distant target as seen in Figure 2.

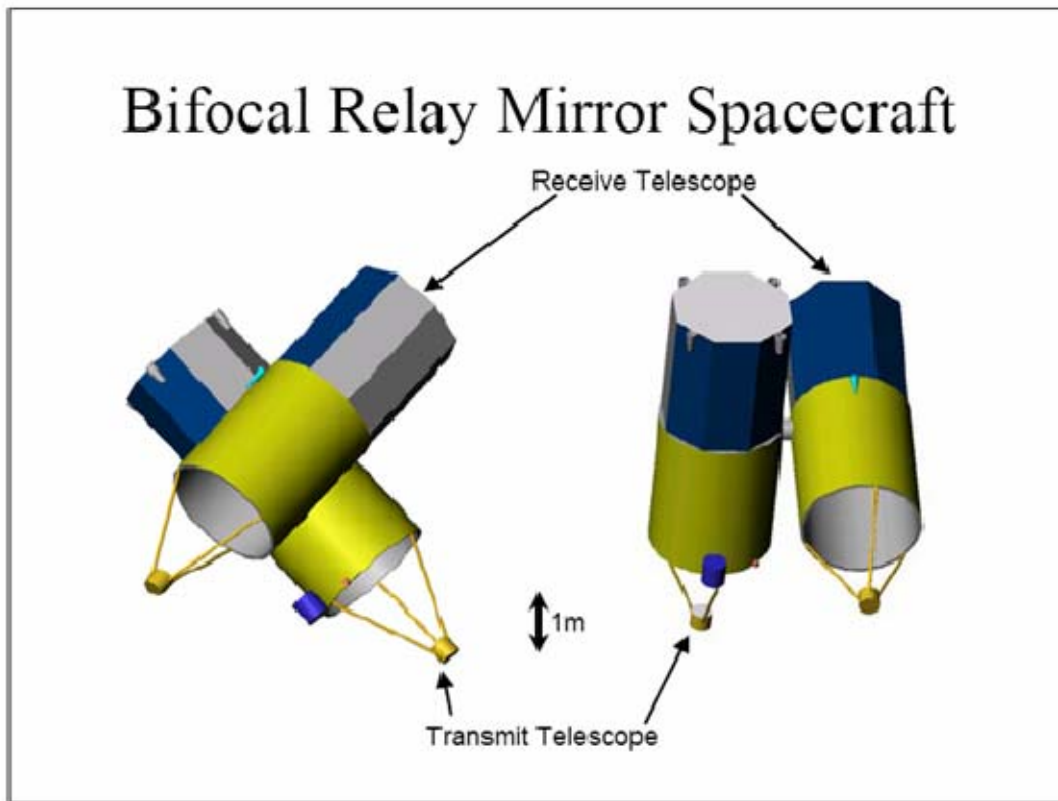


**Figure 2. Bifocal Relay Mirror Spacecraft**

A receiver telescope collects the incoming laser energy and channels it through internal relay optics to a transmitter telescope. The transmitter telescope directs the energy against the desired target as seen in Figure 3.

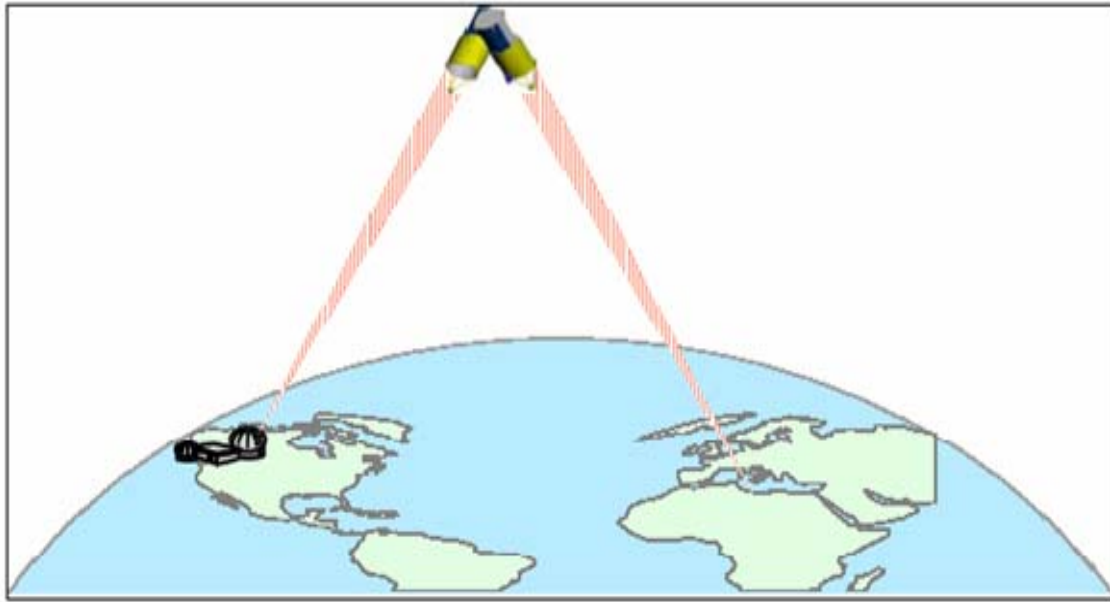


**Figure 3. Bifocal Relay Mirror Operational Concept**

The design specified a target acquisition and tracking systems for each telescope with the transmitter side requiring the added capability of tracking uncooperative terrestrial based targets. The former masters students identified several unique technologies on acquisition, tracking and pointing of laser beam optics that need to be developed prior to operation of this spacecraft.

In December 2000, the NPS Spacecraft Research and Design Center (SRDC) and AFRL submitted a proposal to National Reconnaissance Office for funding to develop these unique technologies for spacecraft purposes. The proposal was awarded in January 2001 and the Bifocal Relay Mirror Laboratory was created at the Naval Postgraduate School. The ultimate goal of the Bifocal Relay Mirror Laboratory is to develop acquisition tracking and pointing of the Bifocal Relay Mirror Spacecraft.

## **B. Thesis Overview**

Chapter II introduces the equipment used for experimental purposes to include the Three Axis Satellite Simulator testbed, Moving Target Source Test Fixture and Extremely Agile Relaying Source Laser. The sensors and actuators, as well as the computer control system will be explained in detail.

Chapter III details the system identification process of the Extremely Agile Relaying Source Laser components. Experimental data will be compiled and mathematically manipulated to form transfer functions for the system components. The mathematical models will be verified by comparing the model to the experimental test results.

Chapter IV explains the control methods used to make various Extremely Agile Relaying Source Laser testbed components operational. A review of the associated control theory will be presented as well as a detail explanation of implementation.

The experimental results and analysis will be presented in Chapter V and the conclusions and recommendations will discussed in Chapter VI.

THIS PAGE INTENTIONALLY LEFT BLANK

## II. EXPERIMENTAL SETUP

### A. THREE AXIS SATELLITE SIMULATOR TESTBED (TASS)

The Bifocal Relay Mirror Laboratory hosts the second generation satellite simulator (TASS2). TASS2 is a test platform used to simulate the Bifocal Relay Mirror Spacecraft. TASS2 consists of a satellite bus and optical payload as seen in Figure 4.

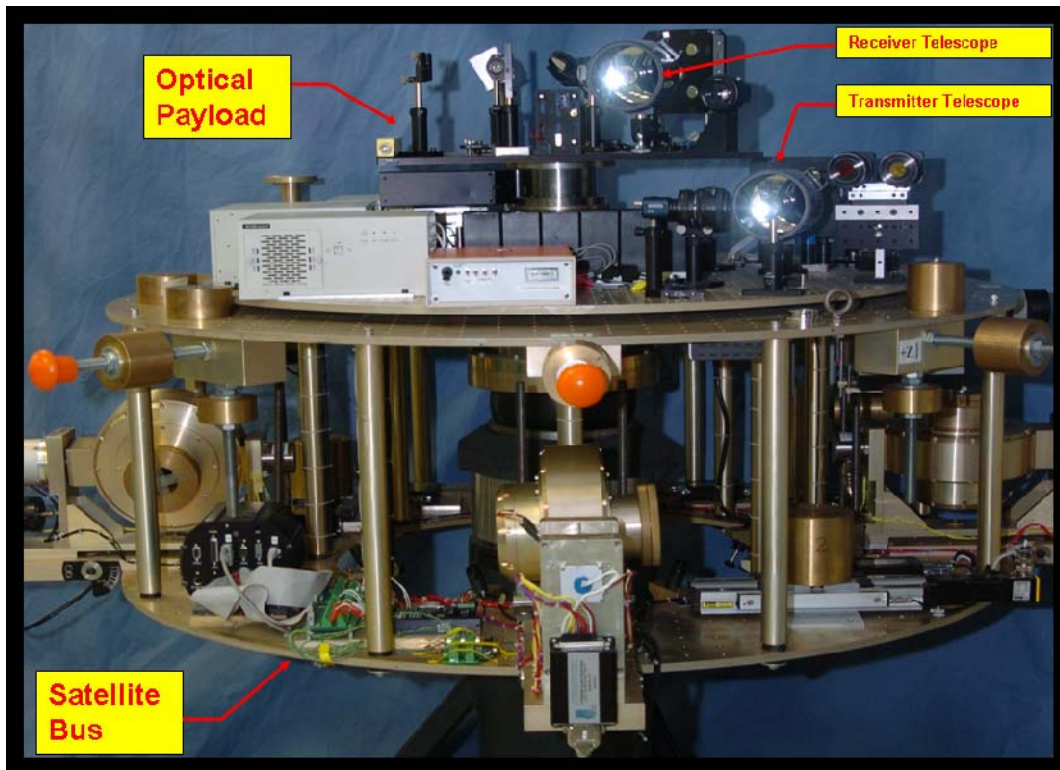


**Figure 4. Three Axis Satellite Simulator #2 (TASS2)**

TASS2 rests on a spherical air bearing which when pressurized, allows the testbed to float in a near frictionless environment simulating extraterrestrial conditions. The satellite bus attitude control is maintained by four single gimbal Control Moment Gyroscopes (CMGs). The CMGs are attached to a hinged frame which allows them to be reconfigured to different skew angles. The satellite bus is balanced by an automatic mass balancing system. Several proof masses are placed around the bus on linear drives allowing both horizontal and vertical motion of control TASS2's center of gravity.



TASS2's optical payload is positioned on a separate deck on top of the satellite bus. The optical payload, as seen in the Figure 5, consists of receiving and transmitting telescopes, two Baker Adaptive Optics fast steering mirrors for jitter control and fine laser steering, a Position Sensing Detector (PSD) that obtains the reference signal, cameras for acquiring the source platform and a Newport optical train components for laser beam routing and alignment.

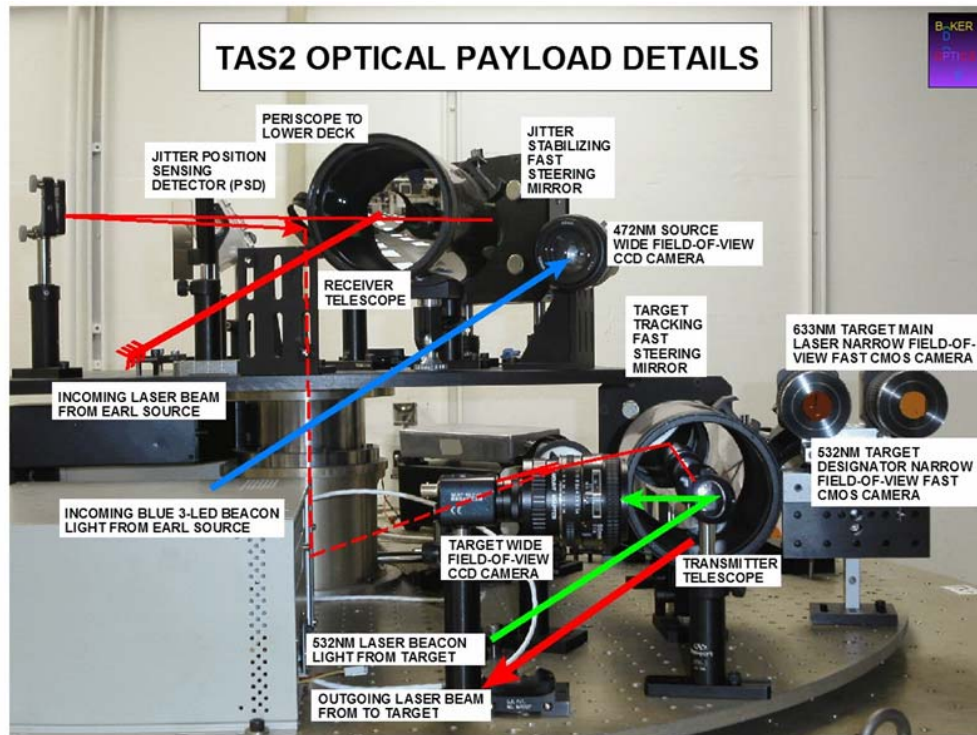


**Figure 5. TASS2 Optical Payload**

The purpose of the optical payload is to receive incoming laser energy from the laser source then redirect the laser energy to a target. The optical payload is also capable of steering the laser source on a moving target as well as negates the effect of jitter using a fast steering mirror (FSM). The payload deck is motorized and can be rotated about the satellite's Y body axis or axis that runs thru the center of rotation to the air bearing. A more thorough explanation of TASS2's hardware can be found in [Kulick, 2004].



## **B. MOVING TARGET-SOURCE TEST FIXTURE (MTSTF).**

The laboratory also hosts a testbed that simulates the laser source and target. This testbed is known as the Moving Target-Source Test Fixture (MTSTF) and can be seen in Figure 6.

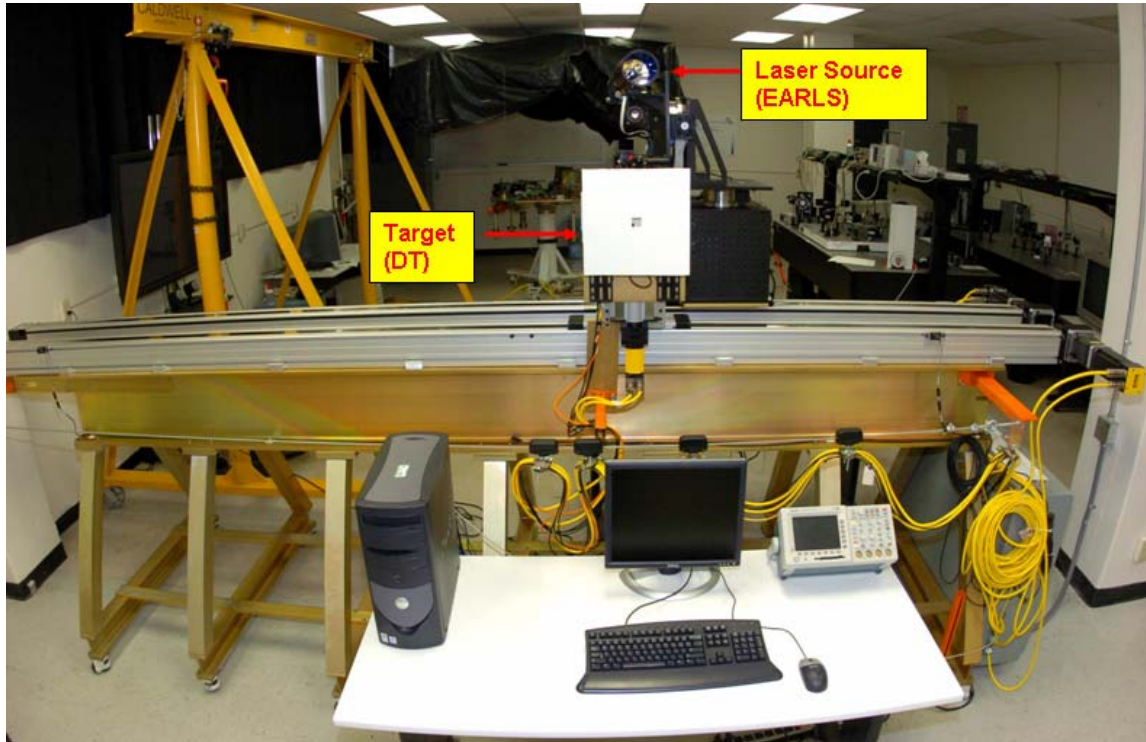


**Figure 6. Moving Target-Source Test Fixture (MTSTF)**

It was designed and built by Guidance Dynamics Corporation and delivered to the BFRM laboratory in June 2005. The MTSTF testbed independently operates the source and target platforms on linear stages or tracks. The source platform was given the name Extremely Agile Relaying Laser Source (EARLS) and the target is called Diagnostic Target (DT).

The idea of MTSTF is to provide a laser source (EARLS) to aim at the satellite (TASS2) while also providing a target (DT) for the satellite to acquire and track as seen in Figure 7.

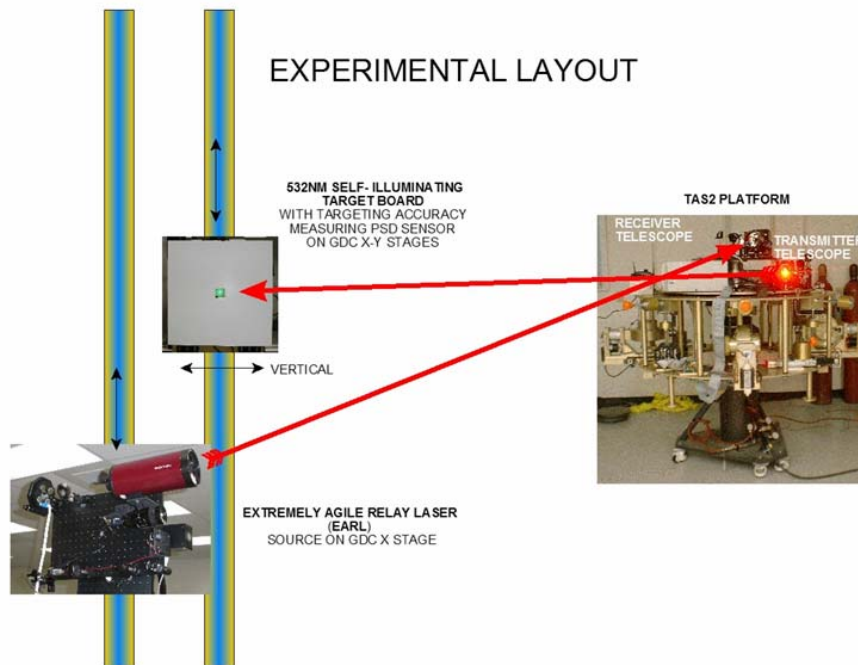


**Figure 7. Experimental Layout**

Since it would be exceptionally difficult to simulate orbiting motion in the laboratory by rotating TASS2 around a laser source, the decision was made to move the laser source with respect to TASS2. So the laser source assembly was placed on a linear motion track permitting it to be moved at a velocity comparable with an orbital rate. The target was also placed on a separate linear track so it may behave in an uncooperative manner. The MTSTF drive components, source components and target components will be explained in more detail below

## **1. Moving Target-Source Test Fixture Drive Components**

### ***a. Linear Track***

The track consists of two independently operated linear tracks as seen in Figure 8.

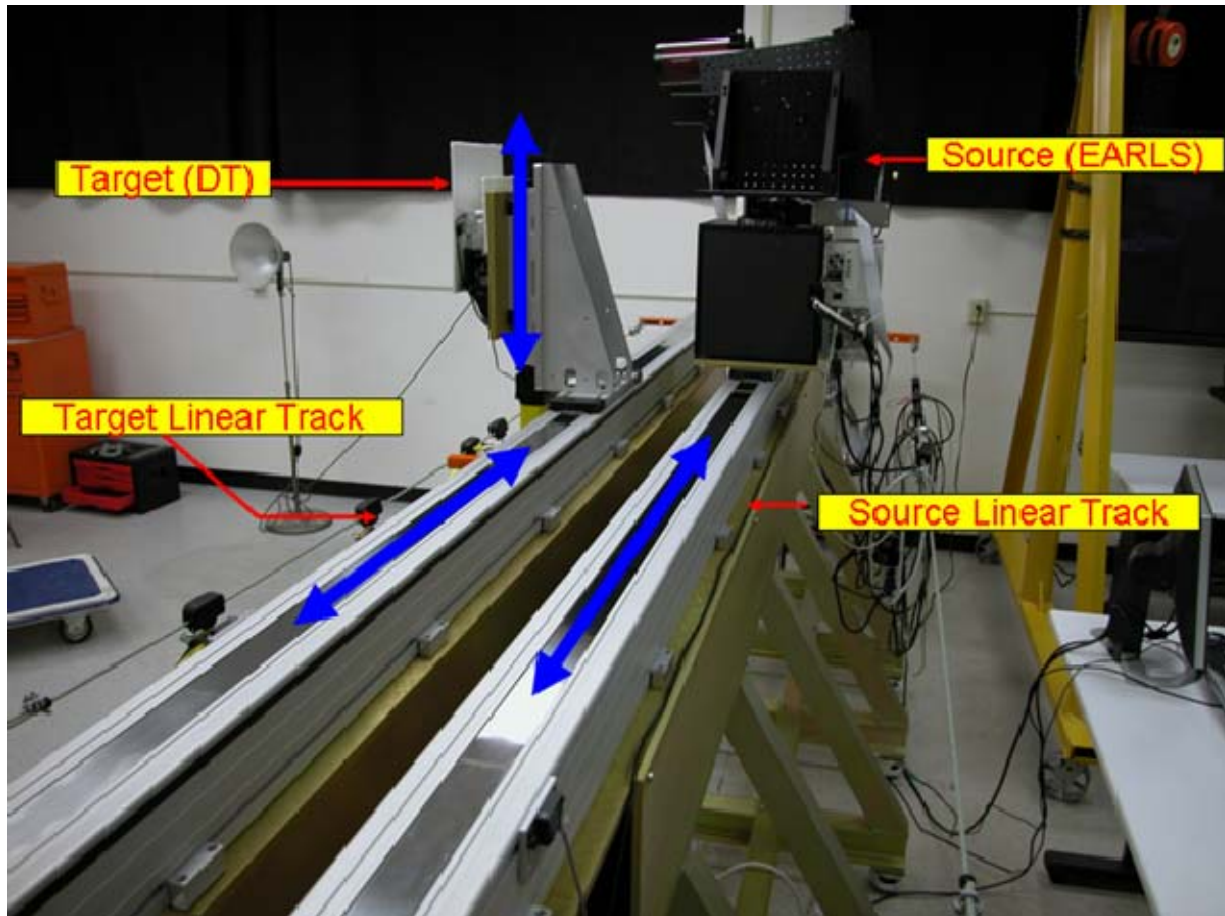


**Figure 8. MTSF Highlighting Independently Operated Linear Actuators**

Both linear tracks are belt driven and manufactured by Parker Hannifin, Model HPLA 120/406XR, Model# 802-7633D. The track has limit switches at each end that results in a software shutdown when tripped. Technical specifications are provided in Appendix A and can be found at:

[http://www.parkermotion.com/products/Belt\\_Driven\\_Linear\\_Actuators\\_5485\\_30\\_32\\_80\\_567\\_29.html](http://www.parkermotion.com/products/Belt_Driven_Linear_Actuators_5485_30_32_80_567_29.html)

***b. Prime Movers***

The prime mover for each linear actuator is a Parker Hannifin J series brushless servo motor, Model# J0922JE-KPSN. The motors are driven by a Gemini GV Series digital servo drive, Model# RS-232/485. Technical Details for the motors are provided in Appendix B and can be found at:

[http://www.parkermotion.com/products/Rotary\\_Servo\\_Motors\\_5208\\_30\\_32\\_80\\_567\\_29.html](http://www.parkermotion.com/products/Rotary_Servo_Motors_5208_30_32_80_567_29.html)

***c. Controller***

The motion for the linear actuator is controlled by a Parker 6K series six axis controller. The controller can be programmed via an attached personal computer which has the Parker Motion Planner software. Technical specifications for the 6K controller are provided in Appendix C and can be found at:

[http://www.parkermotion.com/products/Controllers\\_1745\\_30\\_32\\_80\\_567\\_29.html](http://www.parkermotion.com/products/Controllers_1745_30_32_80_567_29.html)

**2. Extremely Agile Relaying Laser Source (EARLS)**

The principal components of the EARLS assembly are the two motors and optical board for the laser assembly. One motor is for azimuth rotation and the other is for elevation rotation. The laser assembly is mounted on a vertical breadboard which is attached to the elevation motor. The laser assembly is composed of the following major components which can be seen in Figure 9:

1. A New Focus model #9935 optical laser source
2. A Baker Adaptive Optics FSM for jitter control
3. An Orion 102mm optical telescope
4. A Watec video camera for acquiring TASS2
5. And a Newport optical train for laser beam routing and alignment..

## EXTREMELY AGILE RELAY LASER SOURCE (EARL)

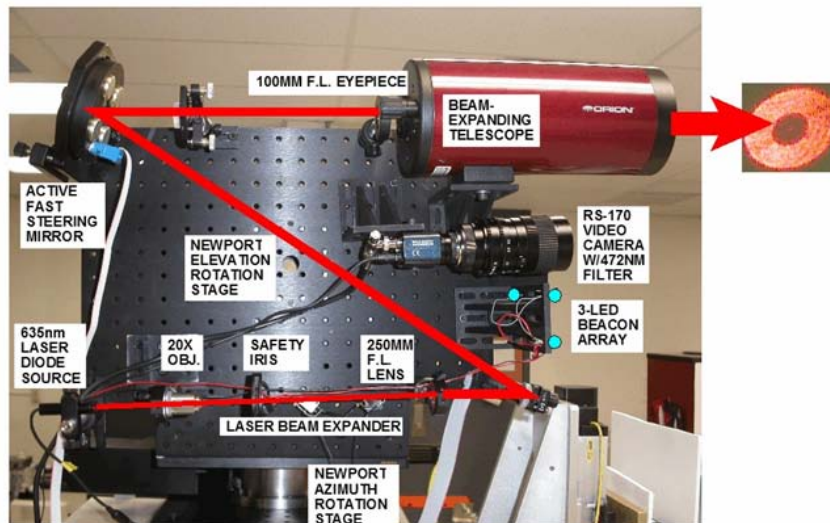


**Figure 9. Extremely Agile Relaying Laser Source (EARLS)**

The laser beam originates at the source and passes through an optical train to the FSM. The laser beam then reflects off the FSM and passes through a beam expanding telescope which forms the beam into a 102mm diameter doughnut shape. Upon departure from the telescope, the laser beam travels to the optical payload on TASS2.



**a. Fast Steering Mirror (FSM)**

The FSM was designed and built by Baker Adaptive Optics as can be seen in Figure 10.

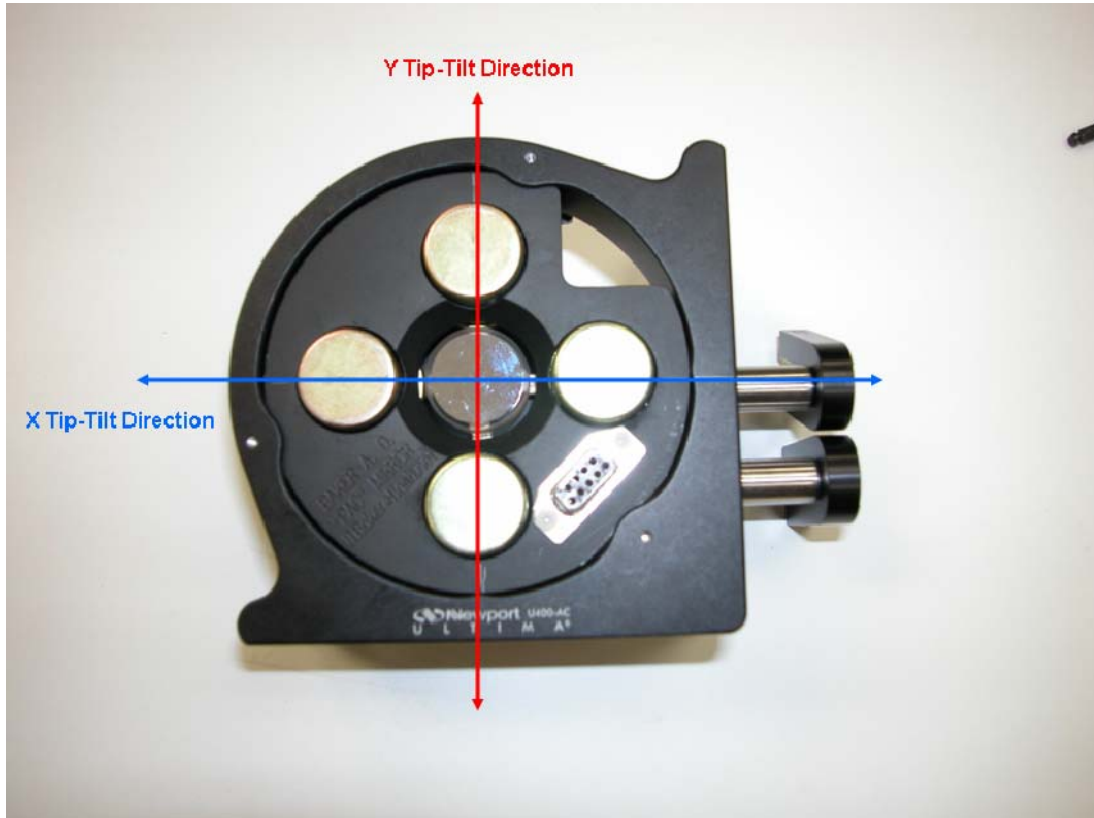


**Figure 10. Fast Steering Mirror (FSM)**

The intent of the source FSM is to eliminate disturbances and vibrations induced by the sources motion along the linear track as well as fine steering of the laser beam. The FSM has a one inch diameter mirror and uses voice coils to position the mirror in response to input commands. The voice coils are placed orthogonally to drive the mirror in the X & Y “tip-tilt” directions. The FSM is driven and controlled by an embedded MATLAB software program. The control bandwidth for the FSM is less than 350 Hz, depending on the direction of motion, and the maximum applied voltage in either direction is 5 volts. Additionally, the natural frequency is approximately 230 Hz depending on the direction of motion.

***b. Video Camera***

The video camera is a Watec Model WAT-902. The camera has a pixel field of view of 811(H) x 508(V) however a field of view of 640(H) x 480(V) is utilized in the experiments. The complete camera specifications can be seen in Appendix D. Mounted on the camera is a Nikon AF Nikkor 50mm 1:1.8 zoom lens to obtain a desired field of view.

The camera captures a black and white image with a MATLAB embedded function. It operates at an update rate of approximately 30 Hz which incidentally makes this device the limiting hardware in the control loop. The camera captures images of a three point LED assembly located on TASS2 for position feedback as seen in Figure 11.

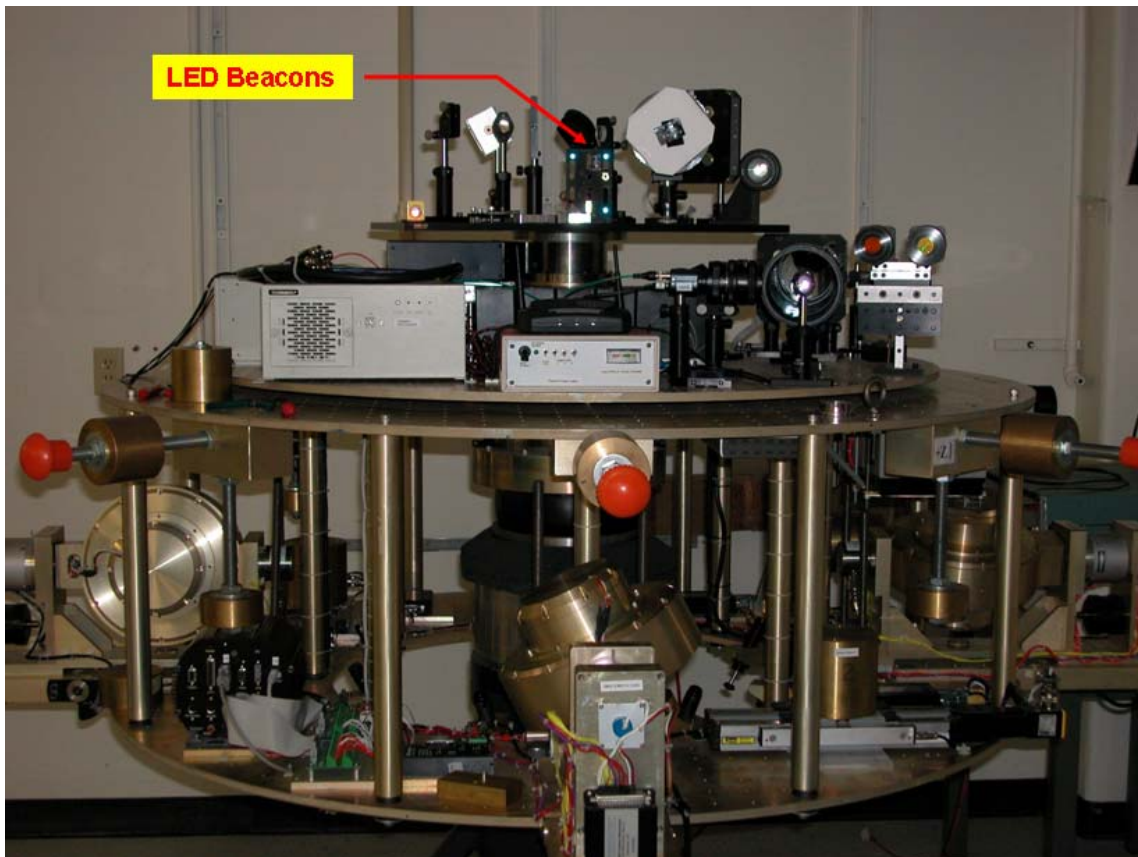


**Figure 11. Location of LED Beacons on TASS2**

*c. Laser Assembly Platform*

The laser source assembly is mounted on a two degree of freedom motorized platform allowing the laser to rotate in both the azimuth and elevation directions. The motors are Newport RV120-MVTP high performance precision rotation stages. These 120mm diameter motors have the capability to travel 360° continuous, however, hardware limit switches are installed on the platform to prevent excess rotation. The motors have an encoder feedback resolution of 0.001°. A CyberResearch mini-PC is mounted on the back of the platform for processing and motor/FSM control.



### III. SYSTEM IDENTIFICATION

#### A. OVERVIEW

Analytically deriving a mathematical model of the laser source and track would have been unreasonably difficult undertaking due to the complexity of the system. Many of the physical characteristics of the system are unknown such as mass, moment of inertia, coulomb and viscous friction and center of mass. Therefore, in this report a simple linear system is considered sufficient in determining the transfer functions of the motors and FSM. Each of these transfer functions was determined through experimental analysis.

#### B. TRANSFER FUNCTION OF AZIMUTH AND ELEVATION MOTORS

##### 1. Mathematical Approach to Determining the Transfer Function

[Chen, 1993] was used as a guide in the following derivation of equations. The DC electric motors were modeled as seen in the Figure 12.

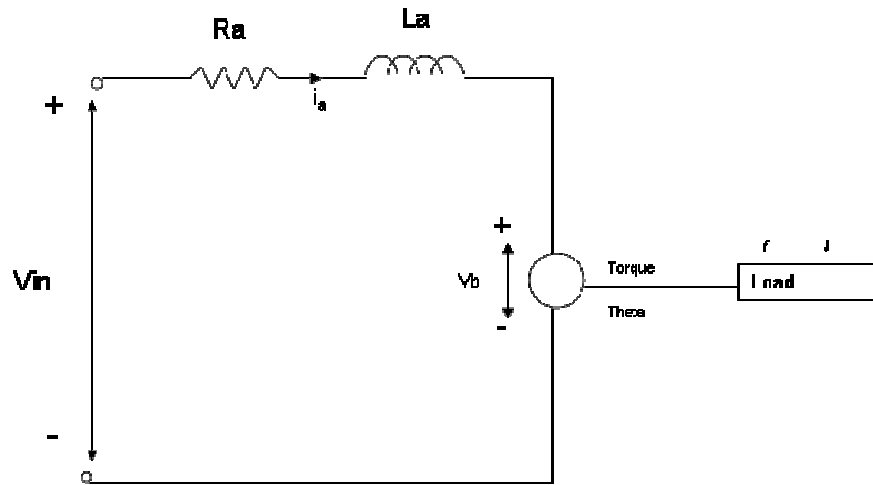


Figure 12. Electrical Schematic of a DC Motor

The torque generated by the motor is given by

$$T(t) = k_t i(t) \quad \text{Equation (2.1)}$$

where  $k_t$  is a torque constant. Due to the external load an electromotive force (back emf) will develop in the circuit to resist the applied voltage ( $V_{in}$ ). The back emf voltage,  $V_b$ , is linearly proportional to the angular velocity of the motor shaft and can be represented as

$$V_b(t) = k_b \frac{d\theta(t)}{dt} \quad \text{Equation (2.2)}$$

Where  $k_b$  is a constant. The motor circuit can be represented by the following equation of motion.

$$Ri(t) + L \frac{di(t)}{dt} + V_b(t) = V_{in}(t) \quad \text{Equation (2.3)}$$

Substituting Equation (2.2) into Equation (2.3) yields

$$Ri(t) + L \frac{di(t)}{dt} + k_b \frac{d\theta(t)}{dt} = V_{in}(t) \quad \text{Equation (2.4)}$$

Now consider the external load which rotates about the motor shaft. The dynamics can be represented as

$$J \frac{d^2\theta}{dt^2} + f \frac{d\theta}{dt} = T_m \quad \text{Equation (2.5)}$$

Where  $J$  is the total moment of inertia of the shaft;  $\theta$ , the angular displacement; and  $f$  is the viscous friction coefficient of the bearing. Substituting Equation (2.1) into (2.5) and taking the Laplace Transform yields

$$Js^2\theta(s) + f\theta(s) = k_t i(s) \quad \text{Equation (2.6)}$$

Taking the Laplace Transform of equation (2.4) and solving for  $i(s)$  yields

$$i(s) = \frac{V_{in} - k_b s\theta(s)}{Ls + R} \quad \text{Equation (2.7)}$$

Substituting Equation (2.7) into Equation (2.6) yields the transfer function

$$G(s) = \frac{\theta(s)}{V_{in}} = \frac{k_t}{s[(Js + f)(R + Ls) + k_t k_b]} \quad \text{Equation (2.8)}$$

Since the electrical time constant,  $\tau_e = \frac{L}{R}$ , is much smaller than the mechanical time constant its effect can be neglected. Therefore,  $L=0$  and Equation (2.8) will become

$$G(s) = \frac{\theta(s)}{V_{in}} = \frac{k_t}{s(JRs + k_t k_b + fR)} \quad \text{Equation (2.9)}$$

Combining terms and converting to bode form produces the first order system

$$G(s) = \frac{\frac{k_t}{k_t k_b + fR}}{s(\frac{JR}{k_t k_b + fR}s + 1)} = \frac{k}{s(\tau_m s + 1)} \quad \text{Equation (2.10)}$$

Where  $k = \frac{k_t}{k_t k_b + fR}$  is the motor gain and  $\tau_m = \frac{JR}{k_t k_b + fR}$  is the motor time constant.

The block diagram of the motors can be represented by the following first order model.

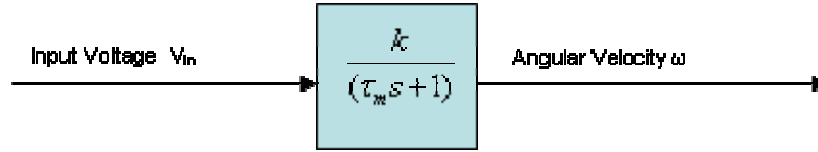


**Figure 13. General Motor Model**

The transfer function from input voltage to output angular velocity is

$$\omega(s) = \frac{k}{(\tau_m s + 1)} V_{in} \quad \text{Equation (2.11)}$$

Taking the inverse Laplace transform yields

$$\omega(t) = kV_{in} - kV_{in}e^{\frac{-t}{\tau_m}} \quad \text{Equation (2.12)}$$

As  $t$  approaches infinity Equation (2.12) becomes

$$\omega(\infty) = kV_{in} \quad \text{Equation (2.13)}$$

The motor gain constant can be determined by applying a voltage ( $V_{in}$ ) to the motor, measuring  $\omega(\infty)$  and using Equation (2.13) in the form  $k = \frac{V_{in}}{\omega(\infty)}$ . Solving for the motor time constant,  $\tau_m$ , in Equation (2.12) produces

$$\tau_m = \frac{-t_0}{\ln(1 - \frac{\omega(t_0)}{\omega(\infty)})} \quad \text{Equation (2.14)}$$

This allows the motor time constant to be calculated by measuring the angular velocity at any transient time,  $t_0$ , and steady state angular velocity  $\omega(\infty)$ .

## 2. Determination of Motor Transfer Functions

In order to establish the motor transfer functions a MATLAB program was written to provide a step input to the motors and read the encoder values. The encoder readings were numerically differentiated to obtain the motor velocity,  $\omega$ , in rads/sec. The motor velocities were plotted as a function of time and  $\omega(t_0)$  and  $\omega(\infty)$  were visually extracted. Using  $\omega(t_0)$  and  $\omega(\infty)$  and the input voltage ( $V_{in}$ ) in the above equations, the transfer functions were computed. The computed transfer functions are presented in Table 1. Computational values used in the calculations can be found in Appendix E.

<b>Elevation Up</b>	<b>Elevation Down</b>	<b>Azimuth Back</b>	<b>Azimuth Forward</b>
$\frac{0.0132}{0.03s + 1}$	$\frac{0.014}{0.03s + 1}$	$\frac{0.0158}{0.03s + 1}$	$\frac{0.0152}{0.03s + 1}$

**Table 1. Motor Transfer Functions**

Figures 14-17 show the actual system response and transfer function response to a step voltage command. The “noise” present in the measured data can be attributed to effects of numerical integration. From these plots the conclusion can be drawn that the calculated transfer functions accurately represent the motors for modeling purposes. The MATLAB Program used for determining the transfer function can be seen in Appendix F.

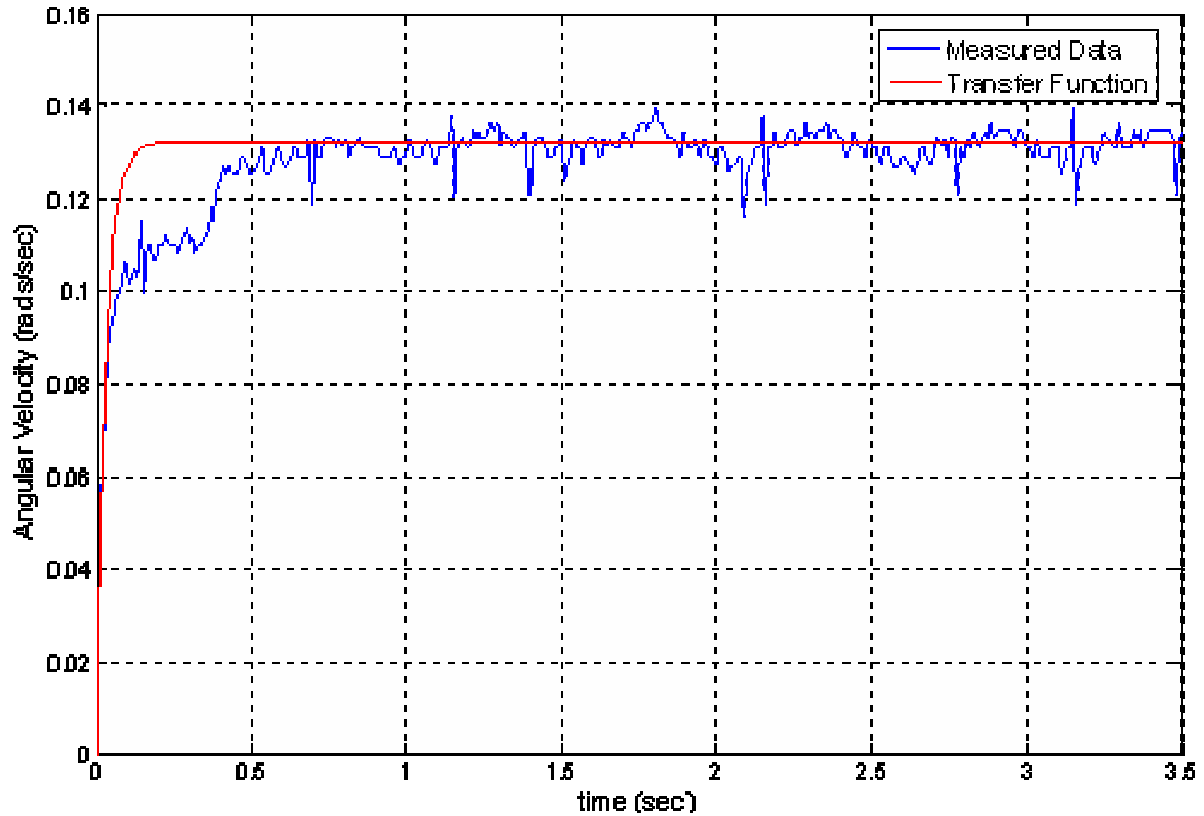


**Figure 14.        Elevation Motor Velocity Measurements - Up Direction**

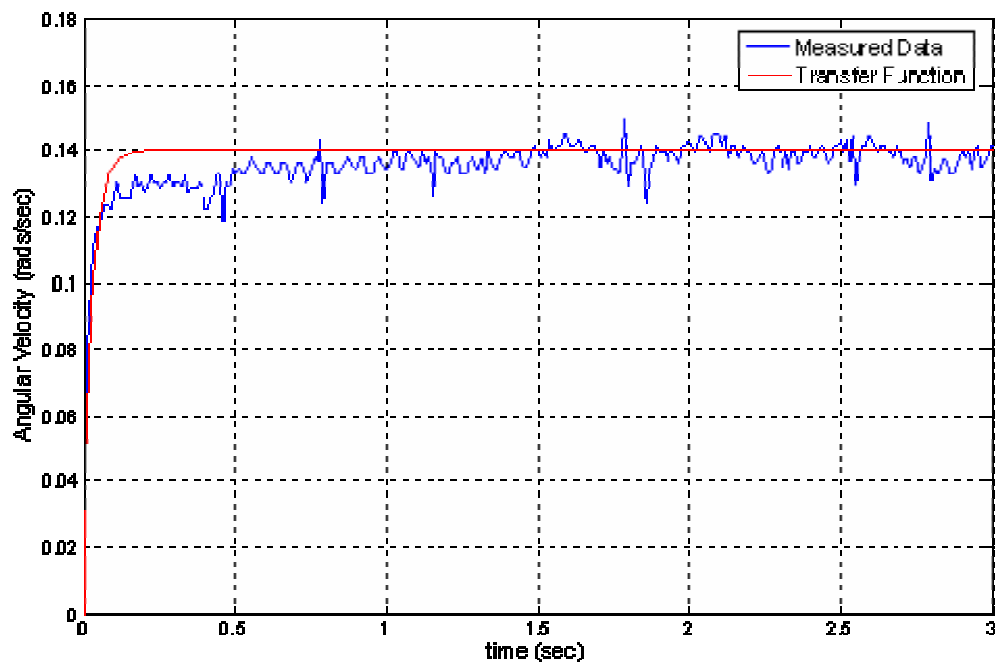


**Figure 15. Elevation Motor Velocity Measurements - Down Direction**

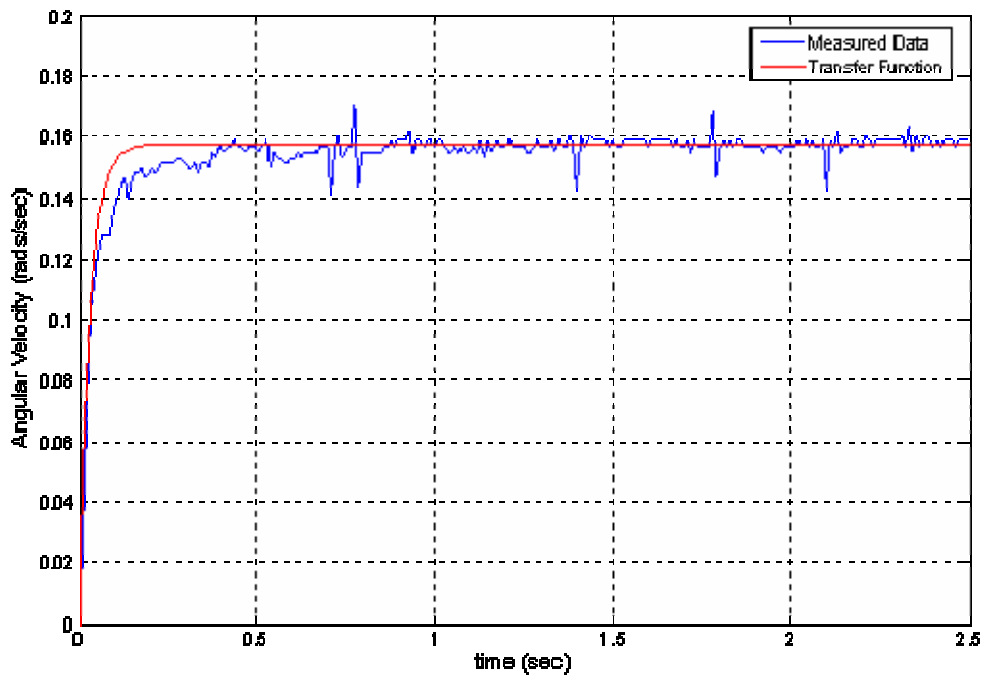


**Figure 16. Azimuth Motor Velocity Measurements - Back Direction**

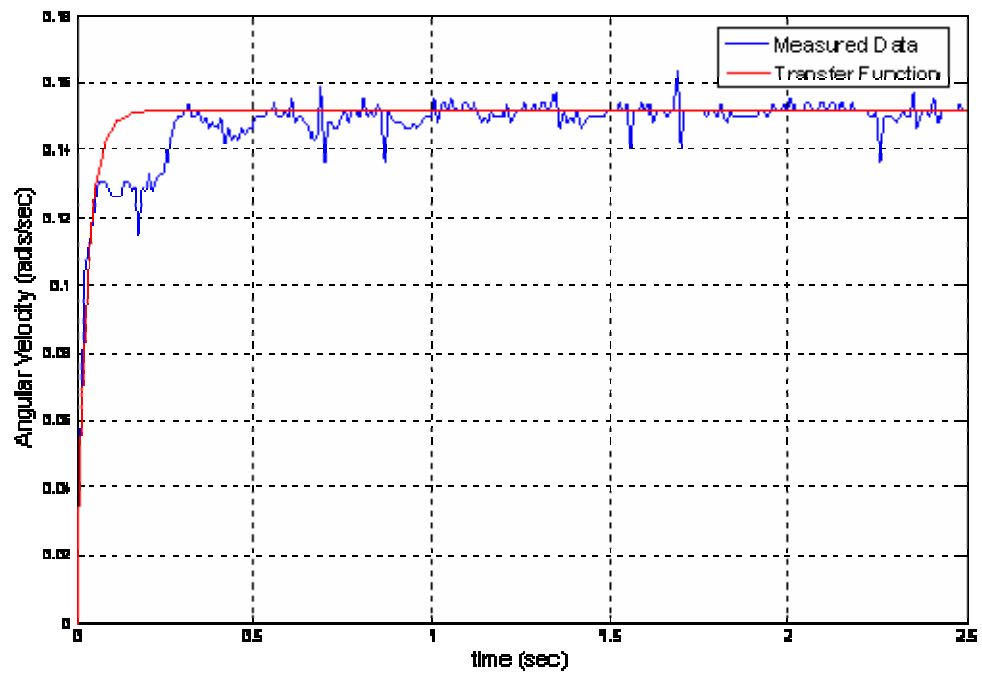


**Figure 17. Azimuth Motor Velocity Measurements - Forward Direction**



### C. TRANSFER FUNCTION OF FAST STEERING MIRROR

In order to determine the transfer function of the FSM, it had to be physically removed from the laser source and placed on the Laser Jitter Control Testbed (LJC) for experimental testing. A Position Sensing Detector (PSD) and laser source were also needed for this experiment. The components were placed in the configuration seen in Figure 8.

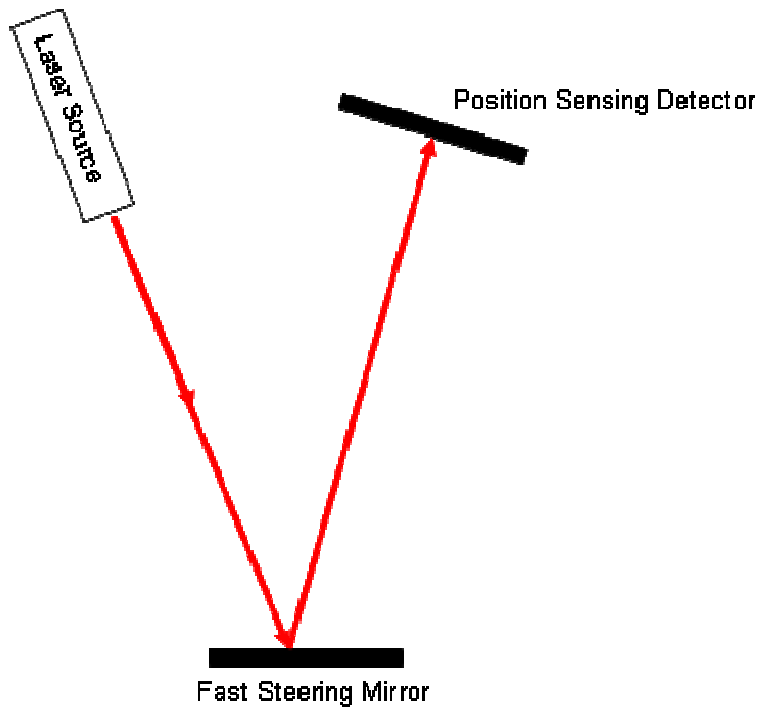


**Figure 18. Fast Steering Mirror Experimental Testing Set Up**

While on the LJC, the FSM was driven by the EARLS computer via a ribbon cable extension. A MATLAB program was written to command the FSM with a chirp signal frequency sweep from 0-800 Hz (see code in Appendix G). The PSD was used to capture the laser's position in millimeters at a sampling time of 0.0005 seconds. So the FSM voltage is the input and the PSD data in millimeters is the output. dSPACE software was used to record and view the raw data from the PSD. The data was then converted to a MATLAB compatible file and the Bode plot was created. Using the methods outlined in [Ogata, 2002, Chapter 8] the transfer function was extracted from the Bode plot.

### 1. Transfer Function for X Tip-Tilt Direction

Using the experimental data the frequency response of the FSM for the X-direction was produced and can be seen in Figure 19.

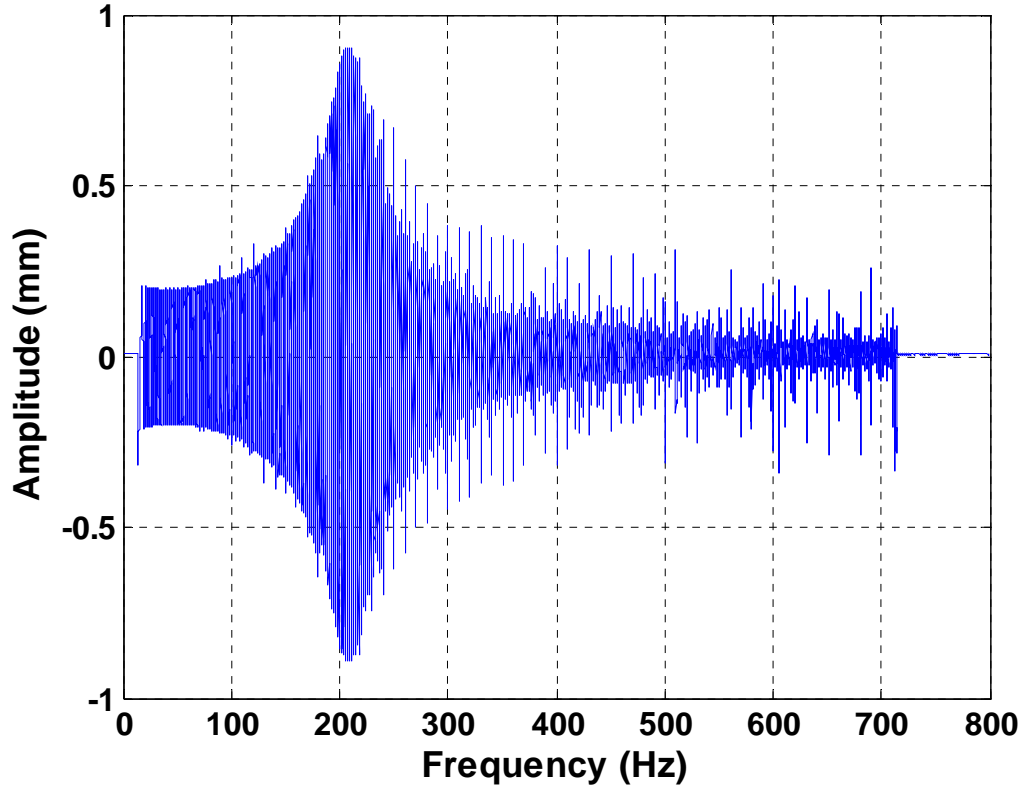


**Figure 19. Frequency Response of Fast Steering Mirror in X-Direction**

The FSM has a natural frequency at 212 Hz. From this data the open loop transfer function was determined to be:

$$G(s)_{x-dir} = \frac{Output(mm)}{Input(volts)} = \frac{0.63}{5.636e^{-7}s^2 + 16.52e^{-5}s + 1}$$

The damping was found to be 0.11.

The Bode plot in Figure 20 compares the actual FSM response to the transfer function confirm that the transfer function closely represents the mirror behavior in the X-direction.

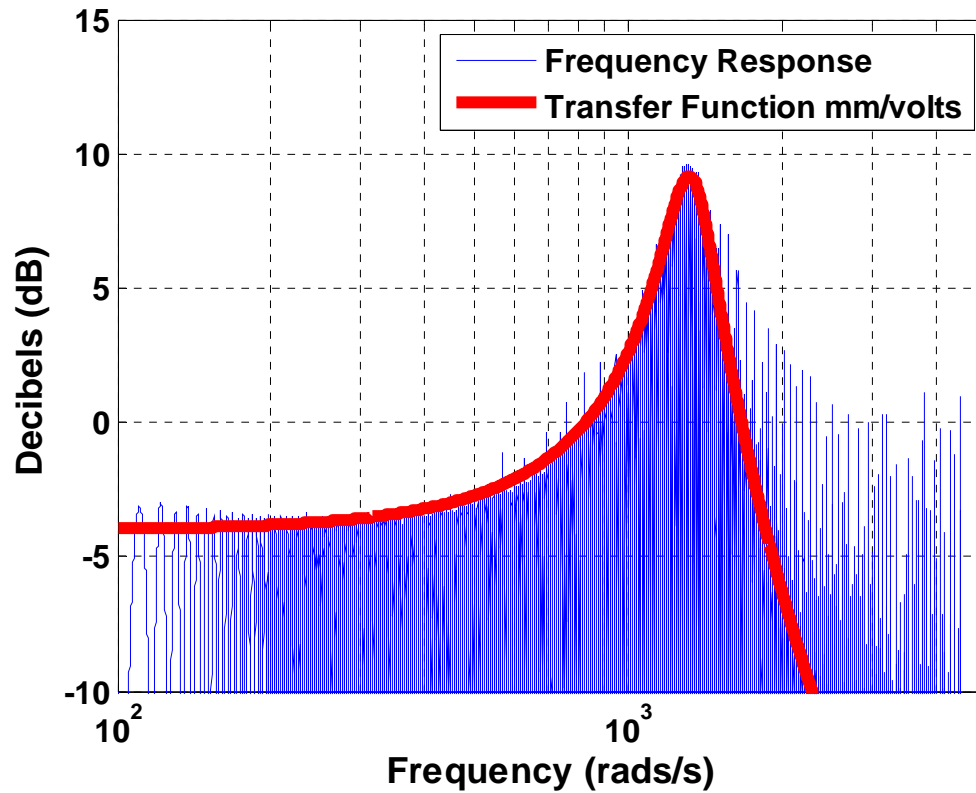


**Figure 20.      Bode Plot of Experimental Data for X Direction**

The Bode plot of the transfer function as seen in Figure 21 shows a bandwidth of less than 326 Hz and a phase margin of  $26^\circ$ .

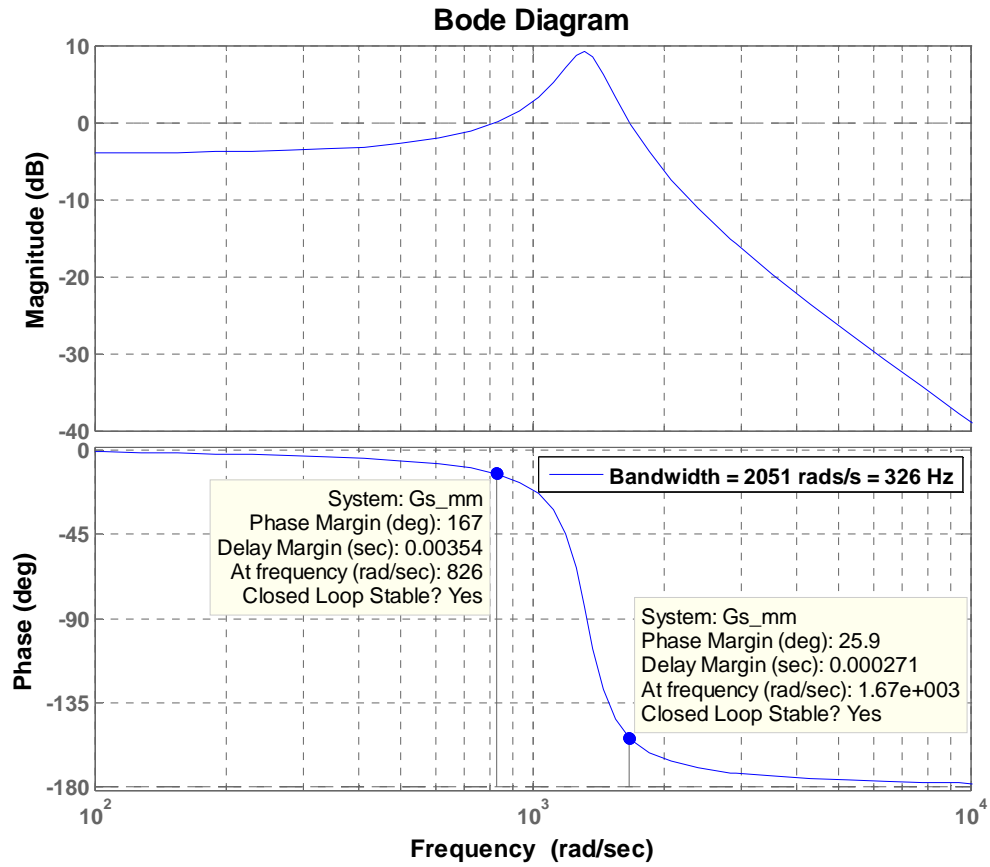


**Figure 21. Bode Plot of Transfer Function for X direction.**

## 2. Transfer Function for Y Tip-Tilt Direction

Using the experimental data the frequency response of the FSM for the Y-direction was produced as seen in Figure 22.

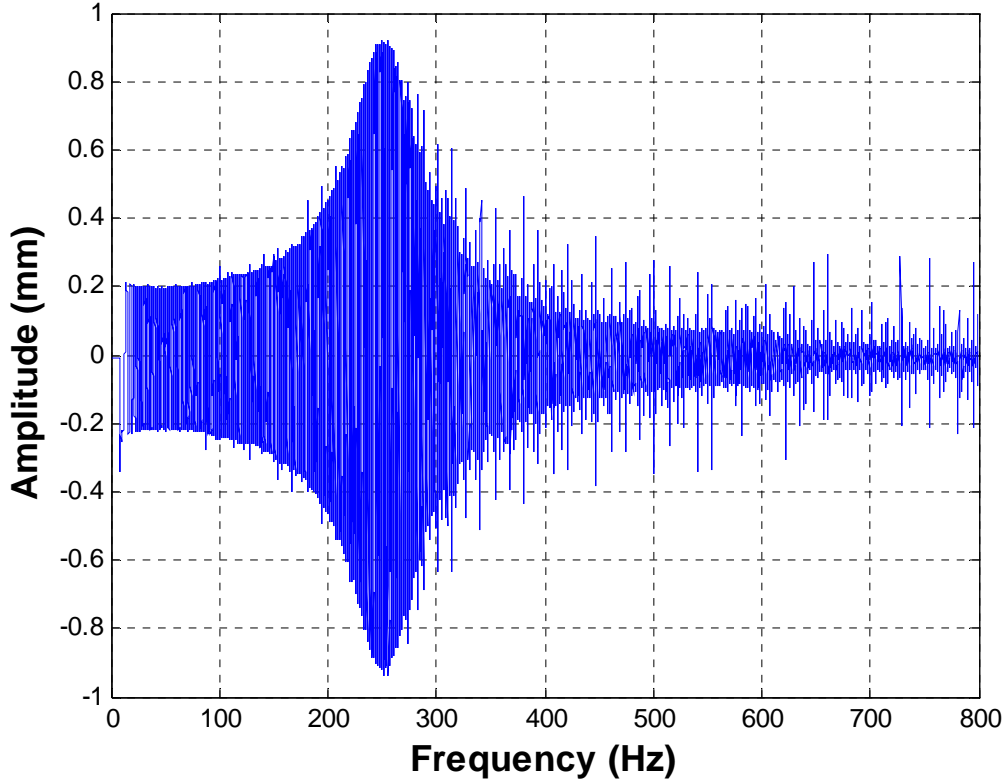


**Figure 22. Frequency Response of Fast Steering Mirror in Y-Direction**

The FSM has a natural frequency at 253 Hz. From this data the open loop transfer function was determined to be:

$$G(s)_{y-dir} = \frac{Output(mm)}{Input(volts)} = \frac{0.68}{3.895e^{-7}s^2 + 13.73e^{-5}s + 1}$$

The damping was found to be 0.11.

The Bode plot in Figure 23 compares the FSM response to the transfer function confirming that the transfer function closely represents the mirror behavior in the Y-direction.

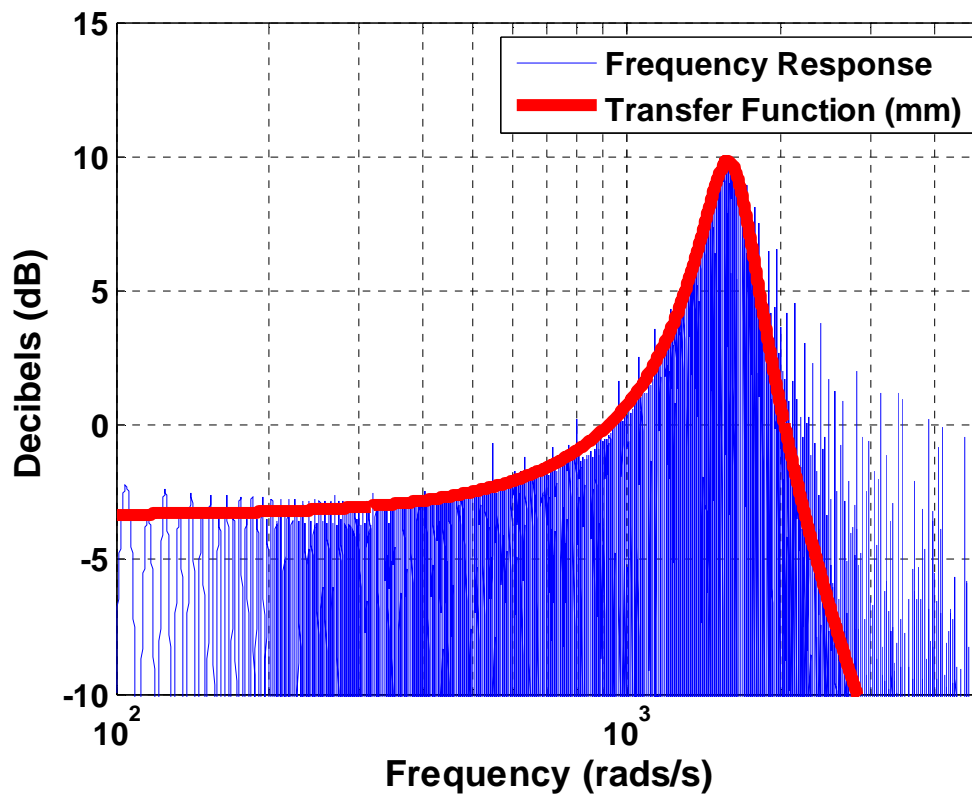


**Figure 23.**      **Bode Plot of Experimental Data for Y Direction**

The bandwidth is less than 393 Hz and a phase margin of  $24^\circ$  as seen in the Bode plot of Figure 24.

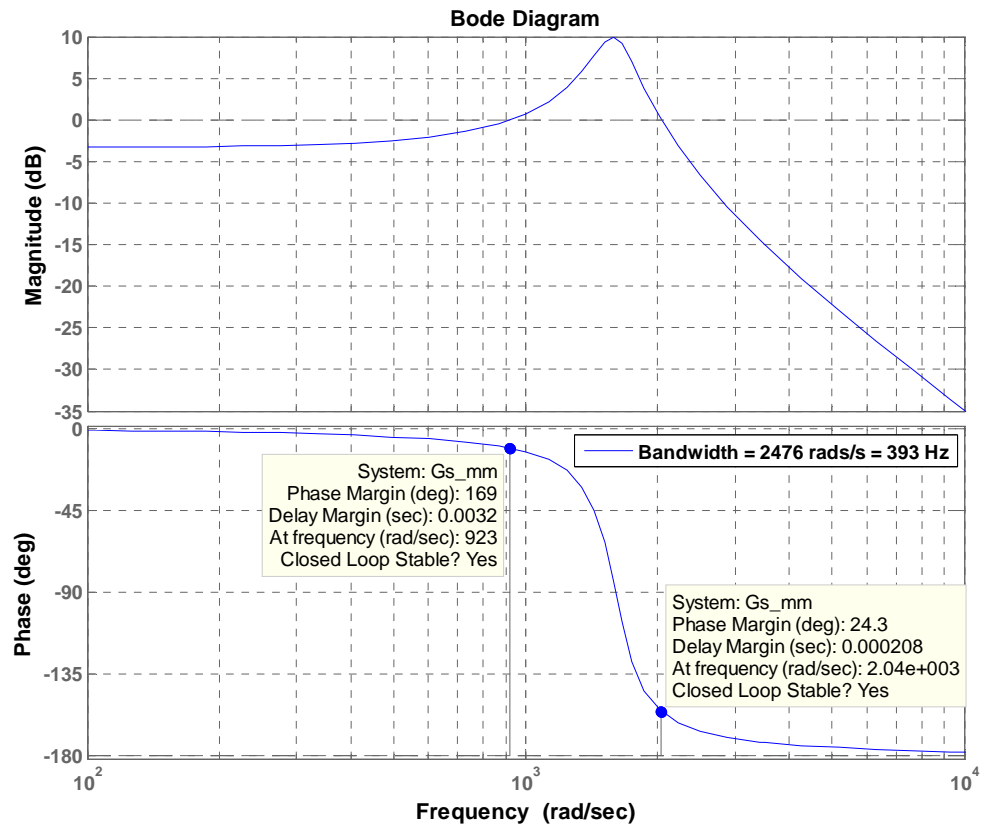


**Figure 24. Bode Plot of Transfer Function for Y direction.**

THIS PAGE INTENTIONALLY LEFT BLANK



## IV. CONTROL METHODS

### A. OVERVIEW

In order to track TASS2 with the EARLS two separate control laws had to be utilized: one for the FSM and one for the motors. Both the motors and FSM are independently operated and therefore separately driven. The elevation and azimuth motors are used to keep the laser source near the receiving telescope on TASS2 but maybe not exactly on target. The FSM is used for disturbance rejection and fine steering the laser beam into the receiving telescope with little or no error. Classical control methods were used for the motor operation while input shaping control was used for the FSM. An explanation of both these methods will follow below.

### B. FAST STEERING MIRROR CONTROL

#### 1. Input Shaping Theory

Since the FSM is solely used for fine pointing of the laser beam there is an implied expectation that mirror has no residual vibrations after a movement. To ensure this requirement is met the “input shaping” control technique was chosen for this system. A description of this technique will be detailed below using the [Singh, Singhouse] input shaping tutorial as a guide.

G.H. Smith first proposed the input shaping technique in which a lightly-damped system, subject to a step input, could generate a non-oscillatory response [Smith, 1956]. This is achieved by exciting two transient oscillations so as to result in beneficial cancellation of the oscillations. For example, if we give a second order system such as the FSM an impulse input, vibrations will ensue. Now if we give the system a second impulse at a specified time later,  $\Delta t$ , the vibration induced by the first impulse can be cancelled. This is illustrated in Figure 25.

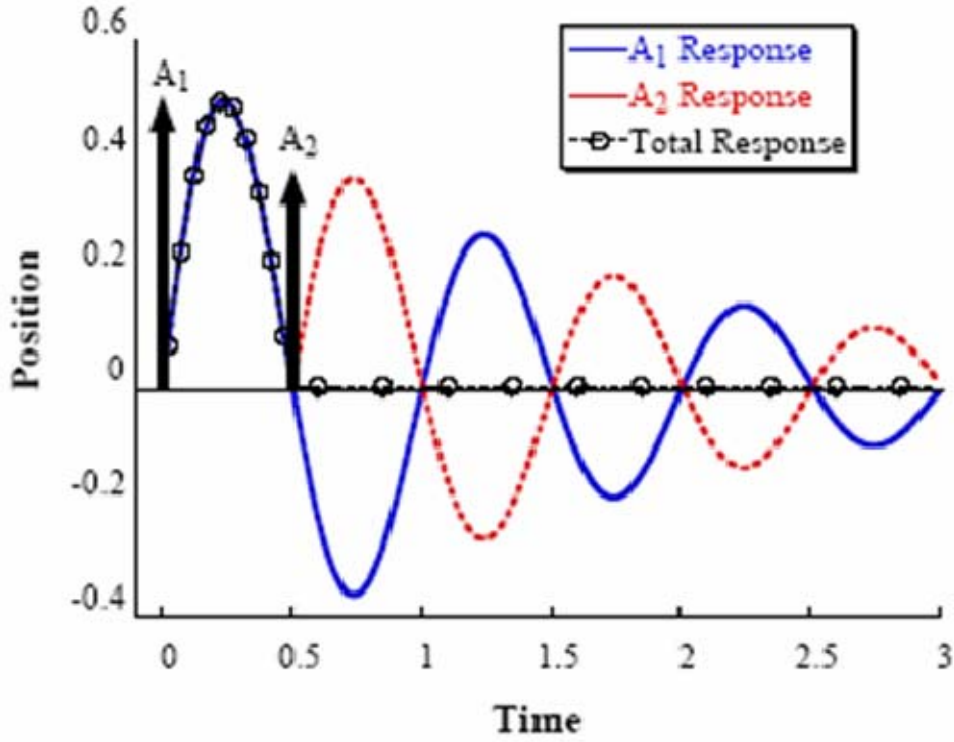


**Figure 25. Two Impulse Response [From Sing, Singhouse]**

In order for this technique to work effectively the amplitudes of the impulses and time locations must be calculated. Assuming that we have an accurate estimate of the FSM's natural frequency in rads/sec,  $\omega$ , and damping ratio,  $\zeta$ , then the vibration that occurs from the impulses can be described by:

$$V(\omega, \zeta) = e^{-\zeta \omega t_n} \sqrt{C(\omega, \zeta)^2 + S(\omega, \zeta)^2} \quad \text{Equation (4.1)}$$

where,

$$C(\omega, \zeta) = \sum_{i=1}^n A_i e^{-\zeta \omega t_i} \cos(\omega_d t_i)$$

$$S(\omega, \zeta) = \sum_{i=1}^n A_i e^{-\zeta \omega t_i} \sin(\omega_d t_i)$$

$A_i$  and  $t_i$  are the amplitudes and time locations of the impulses,  $n$  is the number of impulses and  $\omega_d = \omega\sqrt{1-\zeta^2}$ . Equation 4.1 physically represents the amount of vibration that will result from a unity-magnitude impulse. So by setting this equation to zero the proper amplitudes and time location can be solved for. However, to avoid the trivial solution of all zeroed valued impulses and to obtain the normalized result, we require the impulses to sum to one:

$$\sum A_i = 1 \quad \text{Equation (4.2)}$$

We also want to require the amplitudes to be positive so:

$$A_i > 0, \quad i = 1, 2, \dots, n \quad \text{Equation (4.3)}$$

For a two pulse sequence, the problem has four unknowns – the two amplitudes ( $A_1, A_2$ ) and the two impulse time locations ( $t_1, t_2$ ). By setting the first impulse time ( $t_1$ ) to zero, the problem reduces to three unknowns. In order for  $V(\omega, \zeta)$  to equal zero,  $C(\omega, \zeta)$  and  $V(\omega, \zeta)$  must equal zero because they are squared in and  $V(\omega, \zeta)$ . Therefore, the impulses must satisfy:

$$0 = A_1 + A_2 e^{-\zeta\omega t_2} \cos(\omega_d t_2) \quad \text{Equation (4.4)}$$

$$0 = A_2 e^{-\zeta\omega t_2} \sin(\omega_d t_2) \quad \text{Equation (4.5)}$$

Equation 4.5 can be satisfied in a non-trivial manner when the sine term equals zero. This occurs when

$$\omega_d t_2 = n\pi \Rightarrow t_2 = \frac{n\pi}{\omega_d} = \frac{nT_d}{2}; n = 1, 2, \dots \quad \text{Equation (4.6)}$$

where  $T_d$  is the damped period of vibration. To cancel the vibration in the shortest amount of time, choose  $n=1$  so:

$$t_2 = \frac{T_d}{2} \quad \text{Equation (4.7)}$$

For this case  $A_1 + A_2 = 1$  therefore:

$$0 = A_1 - (1 - A_1)e^{\left(\frac{-\zeta\pi}{\sqrt{1-\zeta^2}}\right)} \quad \text{Equation (4.8)}$$

Rearranging and solving for  $A_1$  gives:

$$A_1 = \frac{e^{\left(\frac{-\zeta\pi}{\sqrt{1-\zeta^2}}\right)}}{1 + e^{\left(\frac{-\zeta\pi}{\sqrt{1-\zeta^2}}\right)}} \quad \text{Equation (4.9)}$$

Defining  $K = e^{\left(\frac{-\zeta\pi}{\sqrt{1-\zeta^2}}\right)}$ , the sequence of two pulses can be summarized as:

$$\begin{bmatrix} A_i \\ t_i \end{bmatrix} = \begin{bmatrix} \frac{1}{1+K} & \frac{K}{1+K} \\ 0 & 0.5T_d \end{bmatrix} \quad \text{Equation (4.10)}$$

Since it would be impractical to drive a system with only impulses, a more usable form of this technique would be to combine the impulse input with a desired input such as a step command. This can be achieved through convolution of the form:

$$f * g = \int_0^t f(\tau)g(t-\tau)d\tau \quad \text{Equation (4.11)}$$

The input sequence is convolved with the desired input and the convolution product is now the new input that will cause no vibration. This process is demonstrated in the Figure 26 for a desired command that is a pulse and a two sequence impulse.

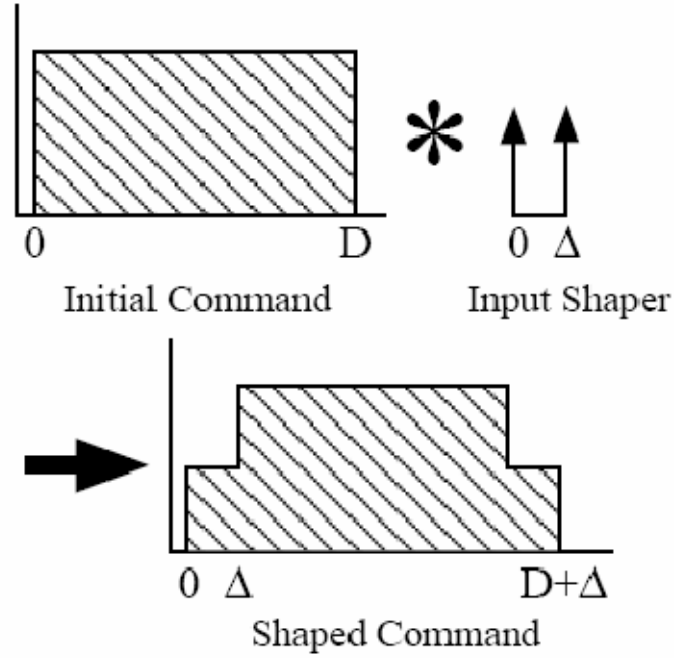


**Figure 26. Continuous Shaped Input [Sing, Singhouse]**

The FSM natural frequencies, damping ratios and damped period of vibrations were ascertained from the system identification process. These values were used in the above equations to calculate the amplitudes and corresponding times for the input. The calculated values can be seen in the Table 2.

	X-Direction	Y-Direction
Natural Frequency, $\omega$	1332 rads/sec	1590 rads/sec
Damping Ratio, $\zeta$	0.11	0.11
Damped Period of Vibration, $T_d$	0.0048 sec	0.0039 sec
Amplitude #1, $A_1$	0.5276	0.5276
Amplitude #2, $A_2$	0.4724	0.4724
Time delay, $t_2$	0.0024 sec	0.0019 sec

**Table 2. Input Shaping Values for Fast Steering Mirror**

To test the effectiveness of input shaping on the FSM performance a SIMULINK model was created for each tip-tilt direction (see model in Appendix H). The model was run with a 0.6 volt step input as well as a 0.6 volts shaped input for each direction. The shaped inputs and FSM response can be seen in Figures 27-30.

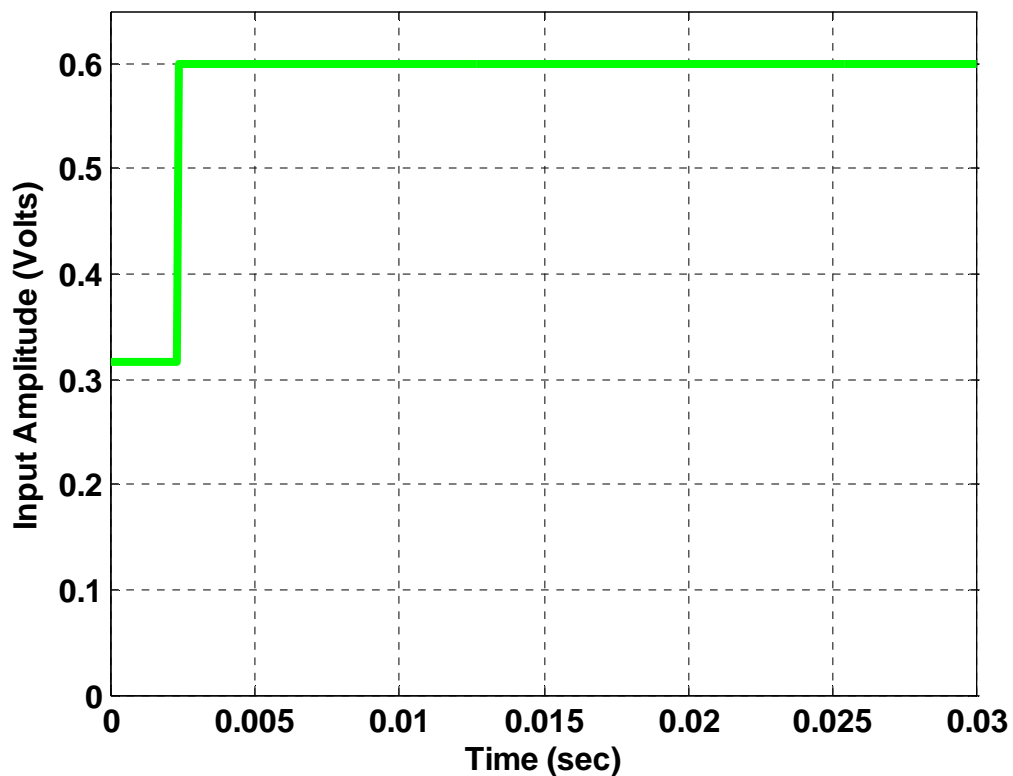


**Figure 27. Shaped Input for X-direction**

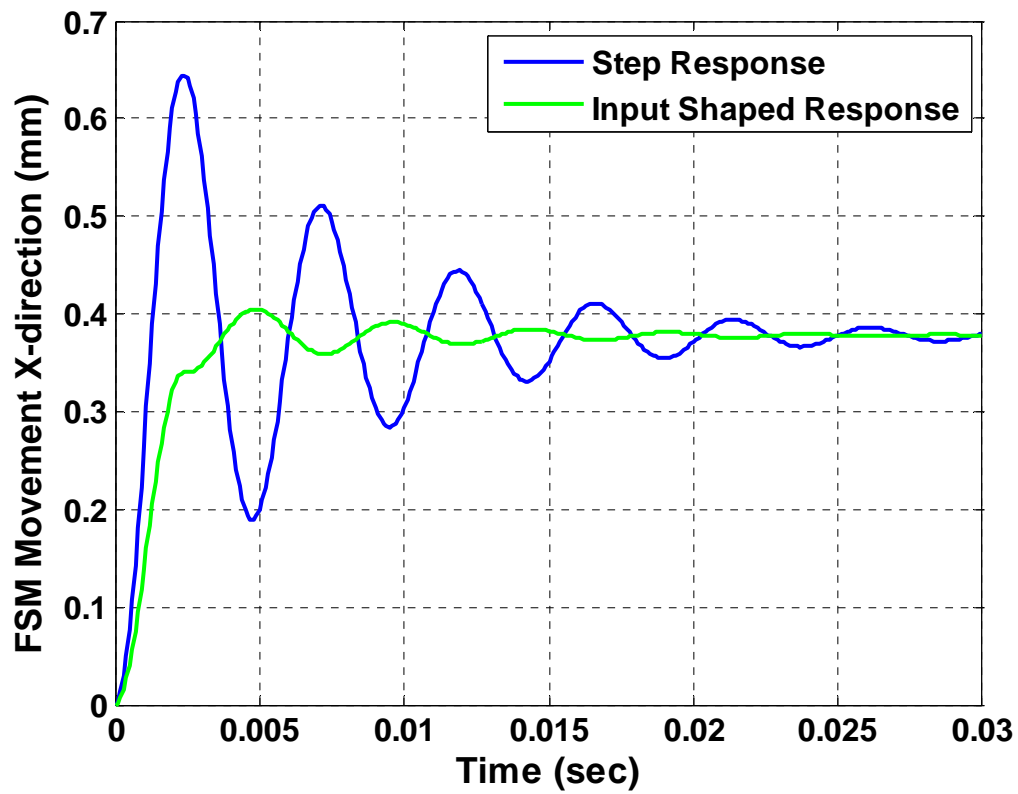
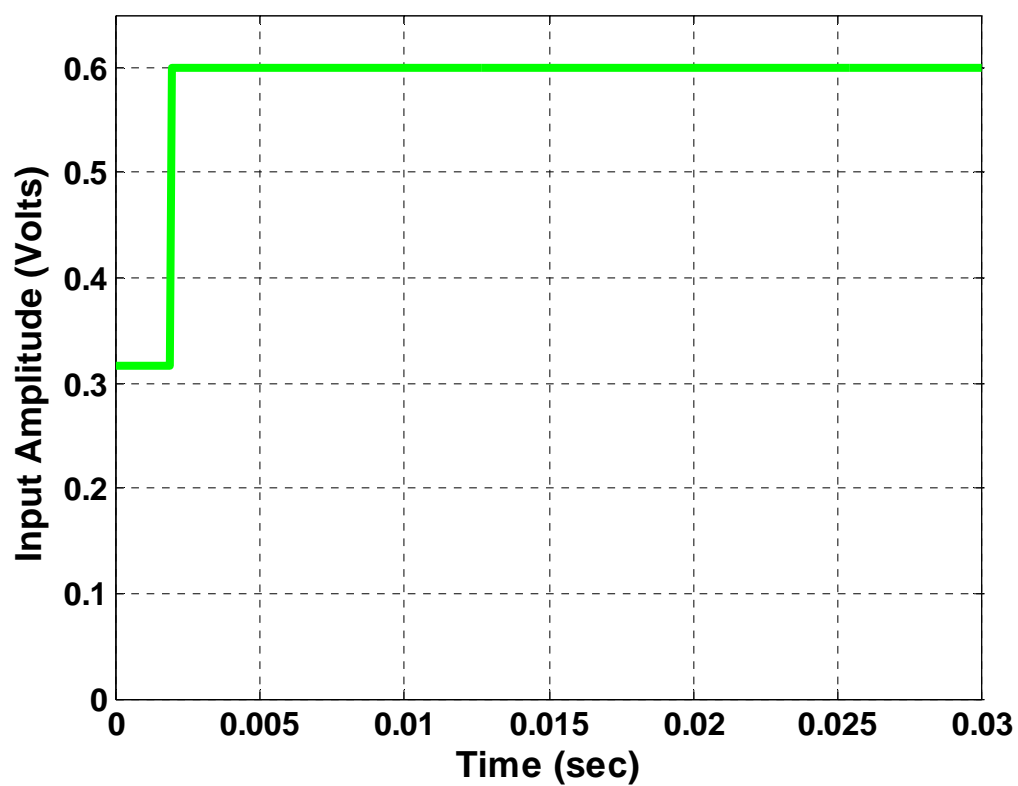
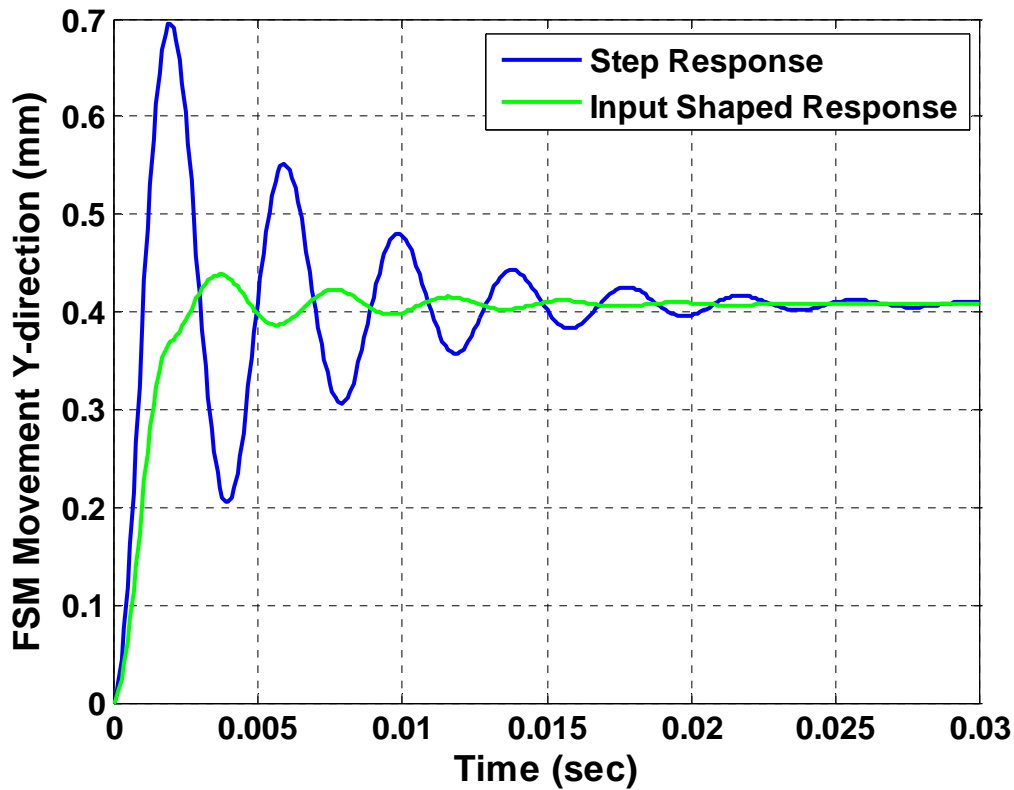


Figure 28. Fast Steering Mirror Response For X-Direction



**Figure 29. Shaped Input for Y-direction**





**Figure 30. Fast Steering Mirror Response For Y-Direction**

There is a significant improvement in both directions with the shaped input; however some slight oscillations still exist. This is likely due to slight inaccuracies in the model. For instance, the damped periods of vibration,  $T_d$ , was taken manually from a plot of the FSM's response to a step input. Also the damping ratio and natural frequencies may not be precise. The disadvantage with the two impulse shaped input is its lack of robustness; it is highly dependant on an accurate model. Nonetheless, the performance is much improved and acceptable for this application.

### C. MOTOR CONTROL

Control of the azimuth and elevation motors was complicated by a combination of motor stiction and uneven loads. The azimuth motor has a stiction breakout voltage of approximately 2.7 volts while the elevation motor has a breakout voltage of approximately 3.6 volts. The values can change slightly depending on the temperature of the motors. Additionally, the EARLS platform has an uneven distribution of mass with respect to the rotation axis of the motors. So the platform was susceptible to rocking motion when the motors go through any change in direction motion. The elevation motor is especially susceptible to rocking motion even with start-stop motion.

To maintain a stable platform and keep the laser on target it was decided that the elevation motor should be used minimally. In fact this was easily done since the EARLS platform moves only along the x-direction on the linear track. Proportional plus Integral (PI) control action was used to control the azimuth motor. To keep the motors from overshooting and having to change direction a deadzone was created to turn off the motors before it overshoot. The ideal magnitude of the deadzone was computed each time the system was run so it varied depending on the current configuration. However, the deadzone was usually around  $\pm 7.6$  pixels (4.3 mm). In another words, when the laser was off target by 7.6 pixel the motors were set to turn off to prevent overshoot. As will be explained in detail later, when the motors turn off, the FSM is still capable of keeping the laser on target. Preventing overshoot was particularly important because the motors never had to change direction and induce vibrations.

Integral control was implemented by summing the pixel error followed by scaling the sum with a gain. To prevent and integral “wind up” while the motors were shut off, the pixel error sum was reset to zero during any operation within the deadzone.

## **V. CONTROL ALGORITHM PROGRESSION**

### **A. OVERVIEW**

A MATLAB program was created to control and move both the motors and FSM. The code can be seen in Appendix I. The control program has essentially three parts: a calibration sequence, a beacon locating sequence and a control sequence. These parts will be explained in detail below

### **B. CALIBRATION SEQUENCE**

As mention previously the camera takes images of the beacons on TASS2 for feedback purposes. The beacons located on TASS2 can be seen in Figure 11 on page 15. When the MATLAB control program is invoked, the motors first move the EARLS assembly to roughly point at TASS2 so that the beacons are within the camera's view. The camera takes an image (640x480 pixels) of the beacons, locates the exact position of each beacon (the beacon location method will be explained later) then labels each beacon either A,B or C based on the distance between the beacons. The camera has a filter placed in the lens that allows it to only capture blue light, therefore only the three blue LED beacons are visible in the image. The beacons appear as white bright spots in the image. Once taken the image would look similar to Figure 31 below. From the known distances between beacons the program computes the number of pixels per millimeter in both the x and y directions on the testbed. This ratio will be used in the control sequence to relate an error in pixels to a physical movement in millimeters. For accurate results, TASS2 should be level during the calibration process. Also the code has a place for the user to define the x and y offset from beacon A to the receiving telescope. The offset is determined by physically measuring the x and y distance (in millimeters) from the beacon to the center of the telescope. These values shouldn't be changed unless the beacon assembly or telescope position has changed. These millimeter offsets are converted to pixel offsets via the aforementioned ratios and used to compute the position of the telescope as illustrated in Figure 32.

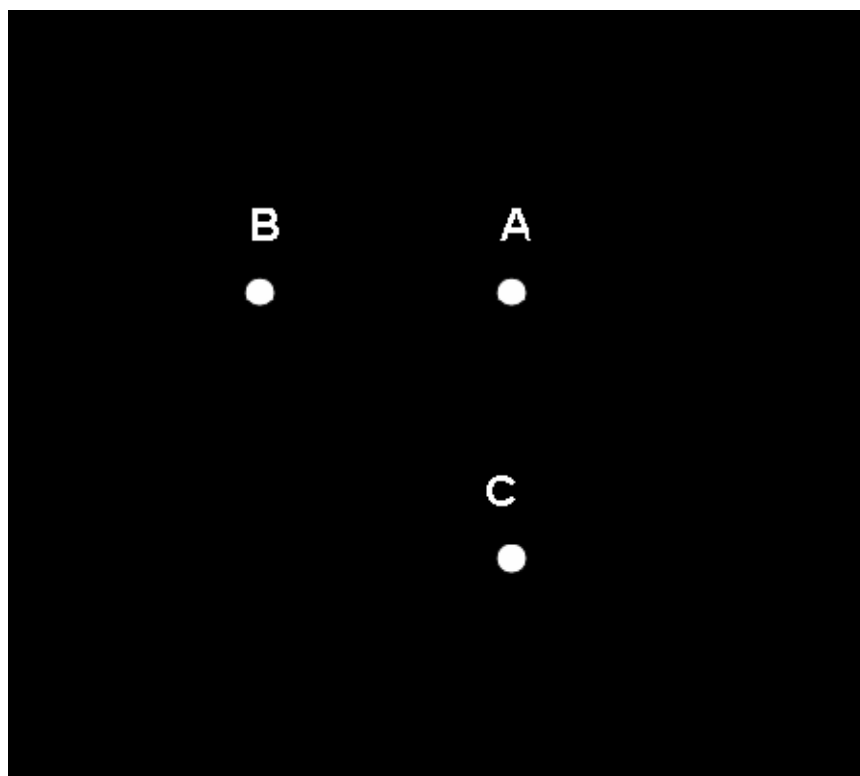


**Figure 31.**      **Cartoon of Camera Image of LEDs**

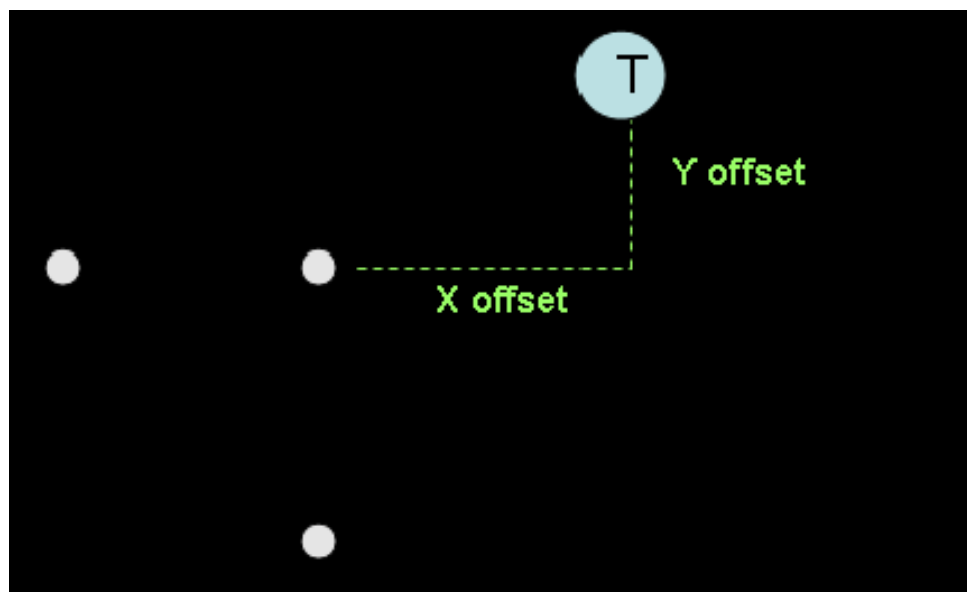


**Figure 32.**      **Cartoon of Camera Image of LEDs with Telescope Location**

Once the receiving telescope position is established the code is capable of accounting for TASS2 rotations in the X-Y plane simply by computing the angle of rotation,  $\beta$ , then measuring the offsets from the A beacon as seen below. The code also has a place to input the laser offset from the make the laser point at the receiving telescope with zero error. This laser offset accounts for the lasers position on the EARLS platform relative to the camera.

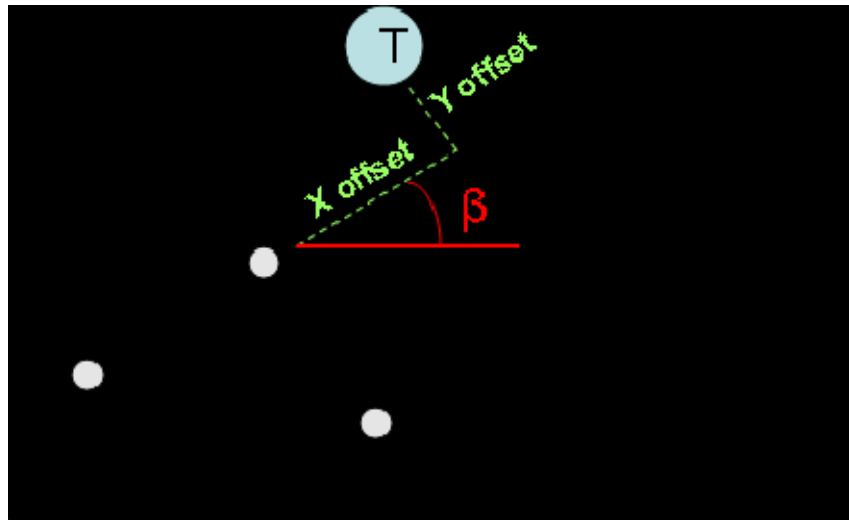


**Figure 33.      Cartoon of Rotated Camera Image of LEDs with  
Telescope Location**

### **C. BEACON LOCATING SEQUENCE**

The beacon locating sequence begins by taking an image of the three beacons. The brightest spot within the image is identified then a virtual box (30x30 pixels) is placed around the spot. Each of the 900 pixels within the box is analyzed and only the brightest ones are retained. The program then takes this cluster of “brightest pixels” and computes the centroid much like computing the center of mass of an object. The resultant centroid is a single point on an image and the x and y position within the image is recorded. Note that the top left corner of the image is the origin of the coordinate frame. Once a LED centroid is marked, all pixels within the virtual box are “blackened out” to prevent it from being used again. This process, referred to as “centroiding,” is repeated until all three beacons are found. Once found the beacons are labeled (A, B or C) by computing the distance between the beacons and comparing to the known pre-measured distances.

### **D. CONTROL SEQUENCE**

After the beacons are marked the program uses the beacons to determine the orientation of TASS2 (i.e. the rotation) and hence the location of receiving telescope. The program then compares the location of the receiving telescope to the laser position and computes the x and y errors. The errors in pixels are used as feedback in the control algorithms so they are converted to voltages via the control methods (PI and Input Shaping). The voltage commands are sent to the motors and FSM to induce movement of the laser. This process repeats at approximately 30 Hz. The Watec camera is the control loop rate constraining hardware since its maximum sample rate is 30 Hz.

Software limiters on the command voltages were placed in the control program to ensure safe and accurate operation. Both motors have a limit of  $\pm 10$  volt references due to the limits of the analog output card. The FSM has a limit of  $\pm 0.60$  volts (15 mm) to keep the laser within the optics range. Test have shown that FSM voltages greater than 0.6 volts induces a movement that drives the laser beam out the transmitting telescope’s optical range resulting in a partially transmitted or “clipped” beam.

## **VI. RESULTS AND ANALYSIS**

### **A. OVERALL RESULTS**

As stated above, the EARLS platform must be calibrated to determine the offsets to make the laser source point at the receiving telescope. The calibration is done when the FSM is at the default or uncommanded position and the offsets are used to determine the error between the laser source and telescope positions through each control cycle. This error will be termed the “sensor error” since the camera is used to produce determine this error. The sensor error is a best estimate from known locations of the laser source point at the receiving telescope since the EARLS assembly doesn’t have the capability to sense the laser beam’s location. This is important because when the FSM is commanded to steer the laser beam, it moves away from the default (uncommanded) position leading to an inaccurate error because the offsets are no longer valid. In short, there is no direct feedback on the laser beam location. To get around this problem an “actual” error was created which takes into account the mirror movement when calculating the error. So the revised object of this project is to keep the laser on target while keeping the actual error to zero. The actual error is computed by converting the FSM voltages to laser distance traveled in pixels then subtracting this movement from the error. The control program computes both the x and y actual error.

Operational testing was conducted by initiating the EARLS control program and allowing it to acquire TASS2. Once this was done the EARLS platform was moved down the linear track to simulate the satellite moving at a constant speed. The x-direction actual errors from an operational test are presented in Figure 34.

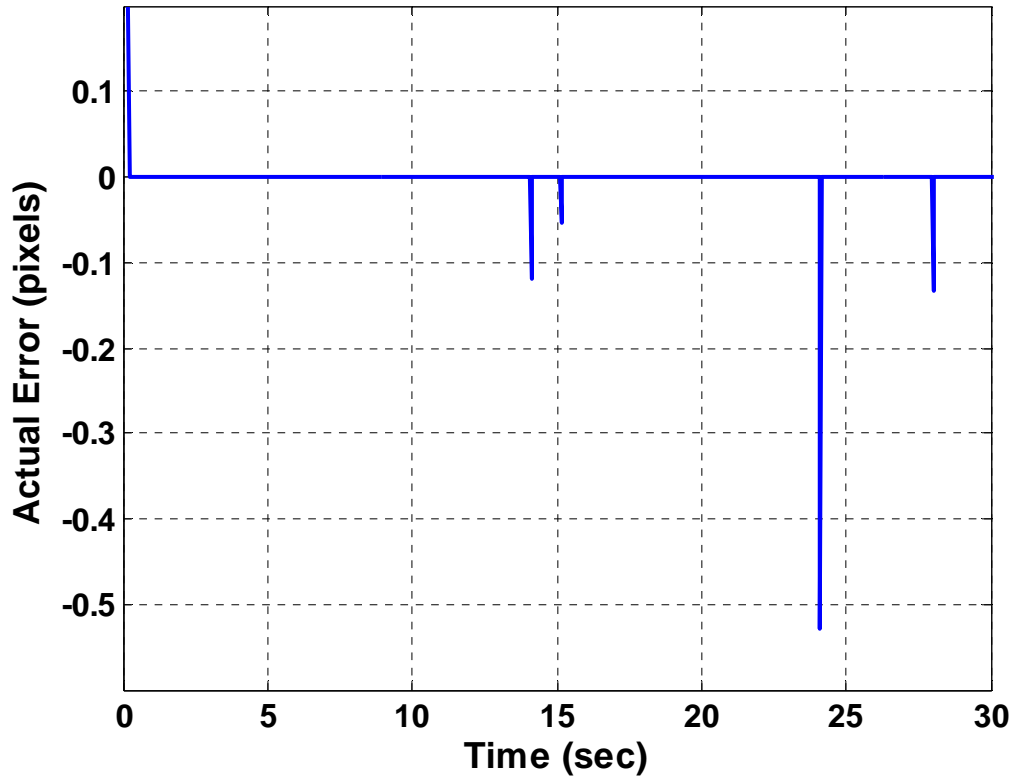


**Figure 34. X-Direction Actual Error**

The error “spikes” are reflective of the laser moving off the target. The greatest error is approximately -0.5 pixels which converts to 0.30 millimeters. This is an acceptable error since the laser beam remain within the receiving telescopes optics.



Figure 35 shows the actual errors in the y direction.

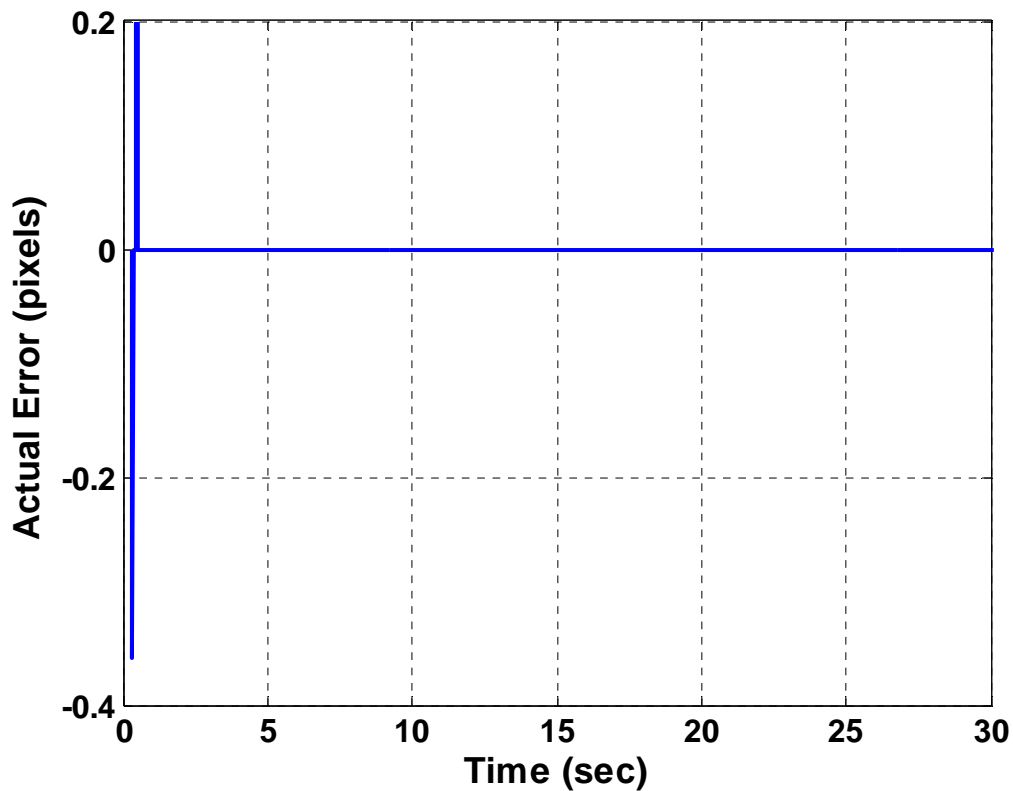


**Figure 35. Y-Direction Actual Error**

Except for the transient segment between zero and approximately one second, which is when the laser is initially moving on target, the y error remains at zero.

## **B. SYSTEM PERFORMANCE IN THE X-DIRECTION**

The control sequences for the FSM and motors are tuned to compliment each other. They are adjusted such that when the error is small enough to be within range for the FSM to correct, the motors turn off. The FSM can generally correct an error less than 7.6 pixels (0.6 volts) in either direction before the laser beam starts to “clip.” Once the error approaches 7.6 pixels the motor turns on and the mirror able to unload.

The x-direction results from an operational test are presented in Figure 36. The figure highlights how the FSM and azimuth motor work together to minimize the actual error.

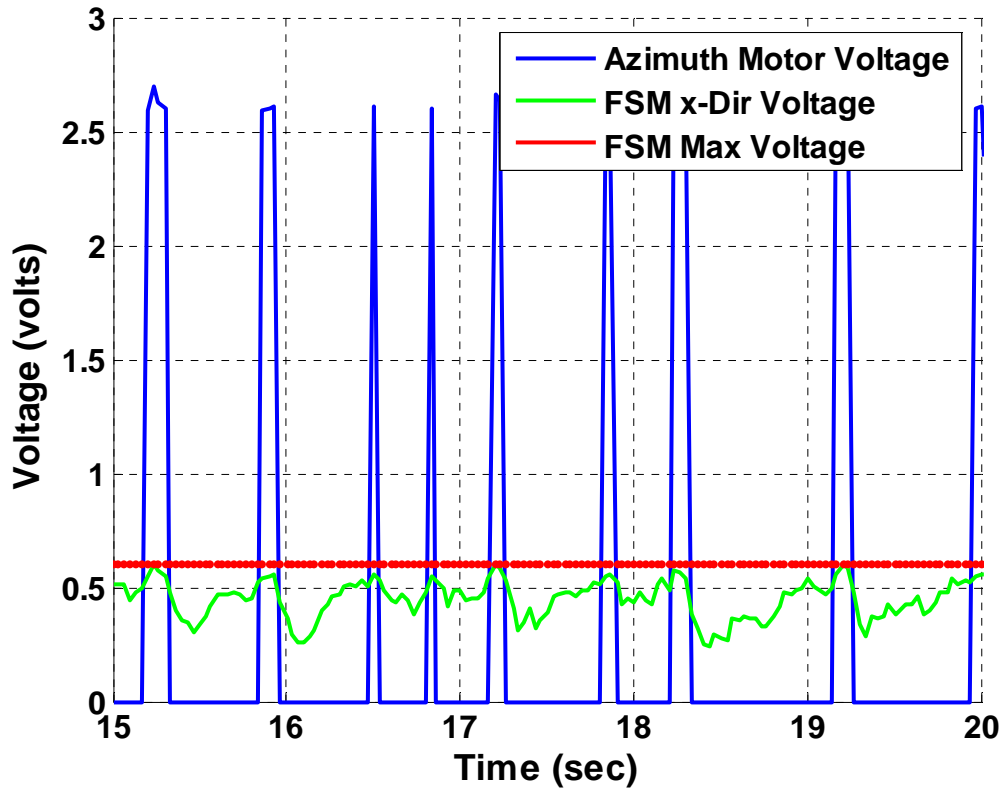


**Figure 36. Azimuth Motor and Fast Steering Mirror Voltages for the X-direction**

This complimentary control has the added benefit of never allowing the laser beam to be clipped (i.e. voltages greater than 0.6 volts) while never allowing the motors to overshoot the target. Additionally, with this type of control sequence, the motors are pulsed in the most ideal manner, slightly above stiction voltage, which doesn't induce excessive vibration.

If the system was performing ideally the FSM correction in pixels should precisely follow the sensor error. Otherwise any deviation between the FSM correction and the sensor error would signal that the FSM wasn't able to account for the error. Figure 37 shows the both the sensor error and mirror movement in the x-direction.

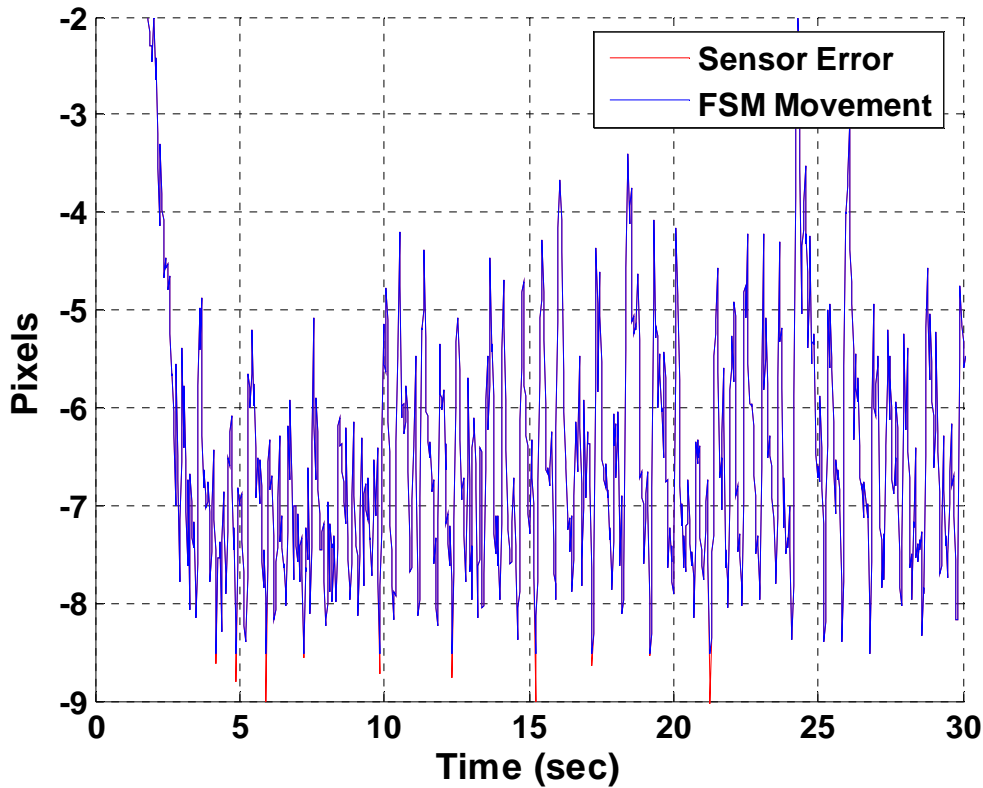


**Figure 37. Comparison Between Error and Mirror Movement in the X-direction**

The FSM correction does follow the sensor error except when the red lines are seen. Consequently, it would be expected that at the point of time when the red lines are visible the actual error would be greater than zero, which is confirmed by viewing Figure 34 in the Overall Results section.

### **C. SYSTEM PERFORMANCE IN THE Y-DIRECTION**

Since the EARLS is moving down a level linear track without changing altitude, the elevation motor is rarely used during operation. As a matter of fact it is desired not to use the elevation motor because it tends to induce excessive rocking of the EARLS. However, the system will have some slight rocking when moving down the linear track so the intent is to correct the y-direction errors induced by this motion with the FSM only. Figure 38 compares the y sensor error to the FSM movement.

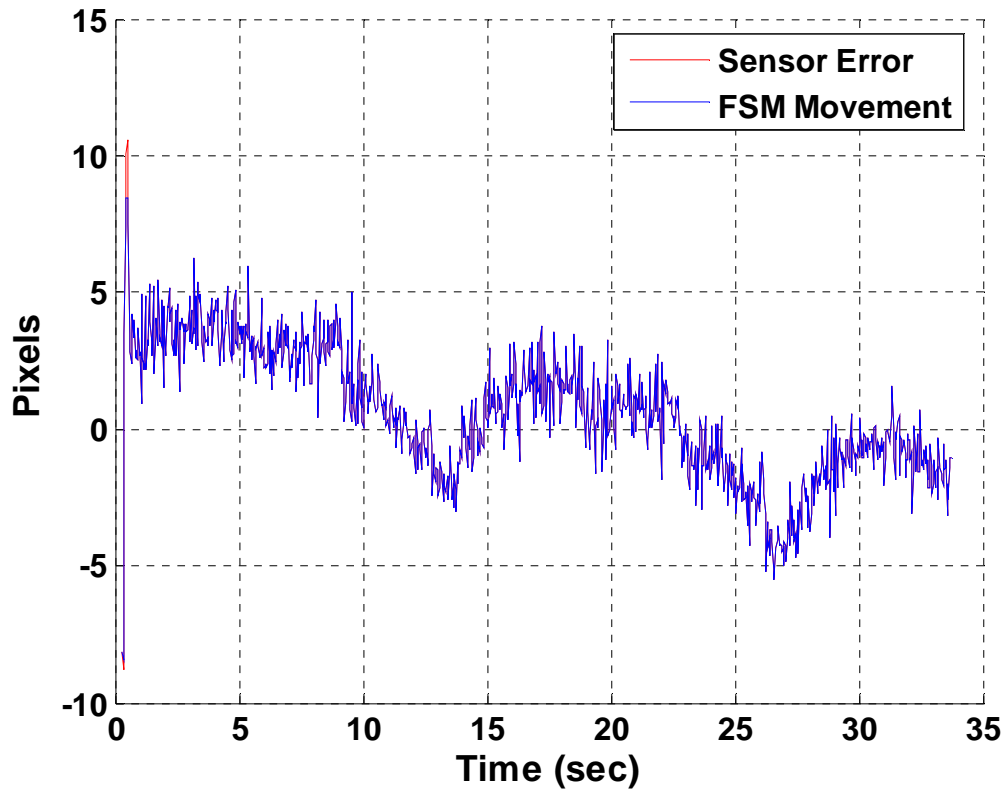


**Figure 38. Comparison Between Error and Mirror Movement in the Y-direction**

Except the initial acquisition of TASS2 there is no deviation. So the FSM is able to correct all the y-direction error. This is also confirmed by Figure 31 in the Overall Results section which shows no actual error. Additionally, the below plot confirms that only the FSM corrects the y error since the motor voltage remains at zero.

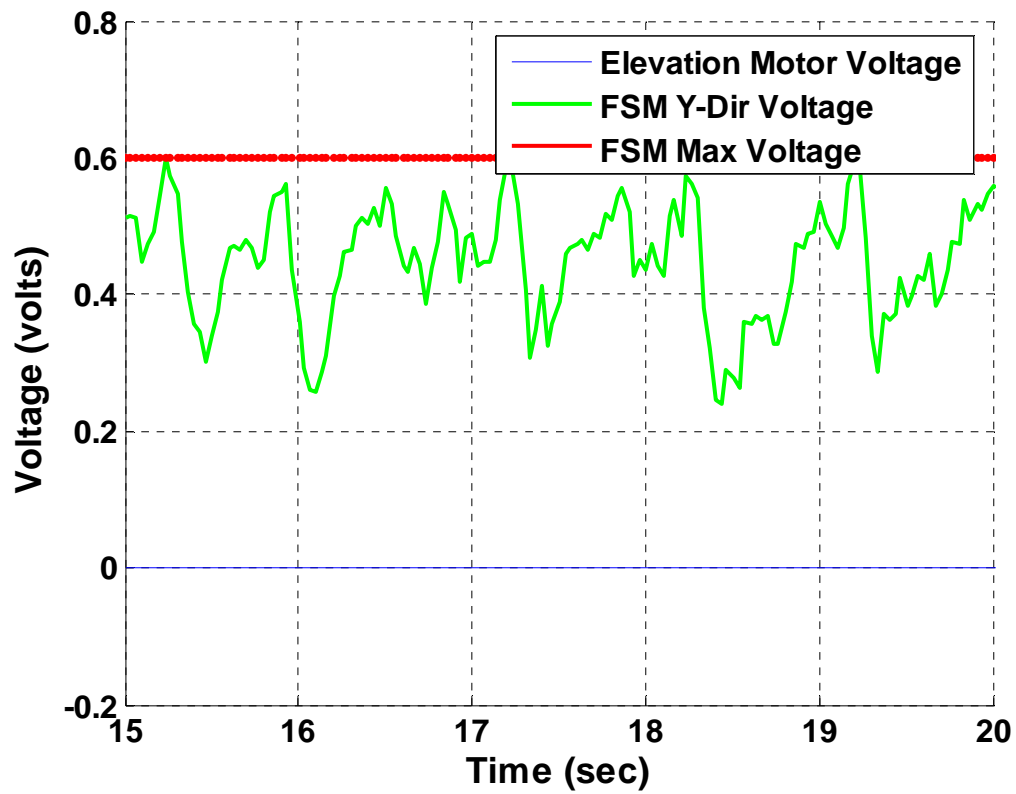


**Figure 39. Elevation Motor and Fast Steering Mirror Voltages for the Y-direction**

THIS PAGE INTENTIONALLY LEFT BLANK

## **VII CONCLUSIONS AND RECOMMENDATIONS**

### **A. CONCLUSION**

The purpose of this thesis was to make the EARLS platform operational by developing a tracking control system. The goal was to point the laser beam at TASS2's receiving telescope and maintain the laser within the telescope's limits in the presence of structural disturbances. To accomplish this two control algorithms were developed, one for the motors and one for the fast steering mirror.

The mathematical model for each motor and fast steering mirror were determined through experimentation then presented in the form of a transfer function. Tracking control methods were developed for these components and implemented into a MATLAB program to form the EARLS control system. The motors were controlled with a proportional-plus-integral control algorithm and the fast steering mirror was controlled with an input shaping algorithm. Operational tests of the EARLS system demonstrated that the control system was able to accurately keep laser source on target within the receiving telescope's limits.

### **B. FUTURE WORK**

Although the tracking system for the EARLS testbed worked exceptionally well, it was only one piece of the overall picture. The EARLS testbed was intended to interact with TASS2's payload which wasn't operational at the time of this theses research. Once TASS2's payload is operational the control system can be refined or new control methods can even be explored. This would be a perfect and meaningful opportunity for a future graduate thesis.

Also, is some equipment upgrades were made the control system would work much more efficiently. As noted previously the Watec video used for feedback has a cyclic limitation of 30 Hz. Replacing this camera with a faster version would open the door to more control opportunities providing higher control bandwidth. Active control of EARLS structural vibrations is also a possibility with the use of vibration sensors on the MTSTF structure. On another note, if the laser beams position on TASS2's testbed could

somehow be fed back to the EARLS control system the FSM control loop could be closed further improving performance.

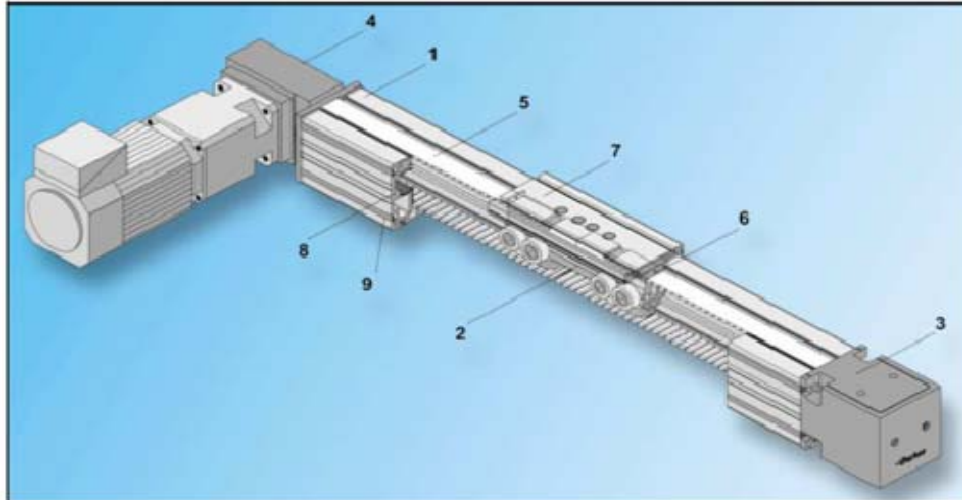


# APPENDIX A: LINEAR TRACK DATA

## Technical data

### 2 Technical data

#### 2.1 Product construction and description



##### The profile (1)

By using finite element analysis we have optimised the aluminium extrusion bar profile to maximise rigidity (torsion and deflection) and minimise weight.

The modular concept permits the same profile to be used for all HPLA variants:

- a) drive version with timing belt drive
- b) version with rack-and-pinion
- c) guide with plastic rollers on aluminium
- d) guide with steel rollers on a steel strip which is integrated into the profile.

6 steel strips (8) are fitted into the profile of the version with steel rollers. The profile can be supplied in cross-sections of:

- 80 x 80mm (HPLA80)
- 120 x 120mm (HPLA120)
- 180 x 180mm (HPLA180).

Two assembly grooves are located on the two sides and on the bottom. These can be used in accordance with DIN-508 for T-nuts to fasten additional mechanical components and to connect several linear actuators. When combined with the covering profile (9), this forms cable ducts, e.g. for the initiator cables.

##### The carriage (2)

The aluminium carriage profile has also been optimised using FEA methods. The plastic or steel rollers (mounted on roller bearings and lubricated for life) are set via the eccentric to eliminate play on all sides. The carriage can be supplied in two sizes as the standard carriage with 12 rollers or extended carriage with 24 rollers.

##### The tensioning station (3)

An easily accessible tensioning station which is simple to maintain and assemble. It is used to set the necessary tension of the timing belt and its alignment (parallel to the pulleys).

##### The drive station (4)

The HPLA can be delivered with numerous drive options. Everything is possible – from the pulley mounted on gearbox shaft through a fully supported hollow shaft up to a drive shaft on left, on right or on both sides.

##### The timing belt (5)

The timing belt is slip-free and is reinforced by integral steel wires, thereby ensuring maximum travel speeds and repeatability.

##### Clamping of timing belt (6)

The timing belt clamping angle and the large area of the clamping guarantees a secure connection between the timing belt and the carriage. The clamping system allows the timing belt to be replaced without the load attachment plate having to be dismantled. This means that attachments do not normally need to be removed.

##### The load attachment plate (7)

The longitudinal grooves integrated on the top of the plate offer many options for the assembly of attachments. When used in conjunction with our clamping profiles, this allows for simple incorporation in a multiple axis system.

Simple and adjustable attachment of operating cams or switch lugs is provided by means of lateral and longitudinal grooves. Height and bolt points are unaffected if the steel strip cover is attached at a later date.

## Technical data

### 2.2 Technical data

HPLA Size	Unit	HPLA080		HPLA120		HPLA180		
		Timing belt drive		Timing belt drive		Timing belt drive	Rack-and-pinion	
		Plastic roller guidance	Steel roller guidance	Plastic roller guidance	Steel roller guidance	Plastic roller guidance	Steel roller guidance	Plastic roller guidance

#### Weight and mass moments of inertia

Weight of base unit with zero stroke								
HPLA with standard carriage (S) as above with steel strip cover	kg	6,0	6,6	18,6	19,8	49,8	53,4	71,8
HPLA with extended carriage (E) as above with steel strip cover	kg	6,8	7,5	20,2	21,6	57,2	61,6	78,4
HPLA with standard carriage (S) as above with steel strip cover	kg	7,8	8,6	23,5	25,2	67,4	72,6	88,6
Carriage + load att. plate (S) as above with steel strip cover	kg	8,6	9,5	25,2	27,1	74,8	80,9	95,2
Carriage + load att. plate (E) as above with steel strip cover	kg	1,5	1,6	5,5	5,7	11,4	11,8	9,9
Carriage + load att. plate (E) as above with steel strip cover	kg	1,7	1,8	5,8	6,0	12,3	12,6	12,5
Carriage + load att. plate (E) as above with steel strip cover	kg	2,4	2,6	8,5	8,9	20,3	21,0	17,2
Weight of drive module	kg	2,6	2,8	8,8	9,2	21,1	21,8	19,8
Weight p. metre of add. length as above with steel strip cover	kg/m	--	--	--	--	--	--	20,0
Weight p. metre of add. length as above with steel strip cover	kg/m	6,0	7,2	13,5	15,4	29,2	33,4	31,4
Mass moment of inertia related to the drive shaft with zero stroke <sup>1)</sup>		6,1	7,3	13,7	15,5	29,4	33,6	31,5
Mass moment of inertia related to the drive shaft with zero stroke <sup>1)</sup>								
HPLA with standard carriage (S) as above with steel strip cover	kgcm <sup>2</sup>	16,0	16,6	136	140	668	695	646
HPLA with extended carriage (E) as above with steel strip cover	kgcm <sup>2</sup>	17,8	18,4	142	146	725	743	698
HPLA with standard carriage (S) as above with steel strip cover	kgcm <sup>2</sup>	23,6	24,7	191	198	1074	1107	793
HPLA with extended carriage (E) as above with steel strip cover	kgcm <sup>2</sup>	25,4	26,5	197	204	1121	1154	845

#### Travel paths and speeds

Maximum travel speed	m/s	5,0						
Maximum acceleration	m/s <sup>2</sup>	10,0						
Maximum travel path, standard-carr. (S/T) <sup>2)</sup> with one profile bar as above with steel strip cover	mm	5610	5590	9560	9530	9440	9400	8880
Maximum travel path, extended carr. (E/F) <sup>2)</sup> with one profile bar as above with steel strip cover	mm	5540	5520	9470	9440	9240	9200	8680
Maximum travel path, standard-carr. (S/T) <sup>2)</sup> with one profile bar as above with steel strip cover	mm	5460	5440	9360	9330	9140	9100	8580
Maximum travel path, extended carr. (E/F) <sup>2)</sup> with one profile bar as above with steel strip cover	mm	5390	5370	9270	9240	8940	8900	8380

#### Geometrical data of guide profile

Cross-section	mmxmm	80 x 80	120 x 120	180 x 180
Moment of inertia I <sub>x</sub>	cm <sup>4</sup>	139	724	3610
Moment of inertia I <sub>y</sub>	cm <sup>4</sup>	165	830	4077
E-module (aluminium)	N/mm <sup>2</sup>	0,72 · 10 <sup>5</sup>		


#### Forces, torques and efficiency

Nominal drive torque	Nm	26,5	74,2	244	58
Maximum drive torque	Nm	47,4	131,4	368	58
Nominal thrust force with fully supported hollow-shaft bearing	N	925	1696	3733	--
Thrust force (effective load)	N	see page 10	see page 11	see page 12	1300
Repeatability	mm	± 0,2	± 0,2	± 0,2	± 0,05
Efficiency	%	95	95	95	80

#### Data of pulley and timing belt

Travel distance per revolution	mm/U	180	270	420	280
Number of teeth on pulley		18	27	21	28
Timing belt width / pitch	mm	25 / 10	32 / 10	56 / 20	42 / 10
Weight of timing belt	kg/m	0,166	0,213	0,550	0,251
Response radius of the pulley of the drive (R <sub>A</sub> )	mm	28,7	43,0	66,8	44,56

- 1) Additional mass moment of inertia due to effective load and weight of timing belt: (see chapter 2.4).  
 2) Longitudinal flange connection can be used for longer travel paths. Some restrictions have to be considered for: maximum load permitted, drive torque, speed, acceleration and Repeatability (see chapter 3.10). For actuators with rack-and-pinion drive the travel distance is unlimited (as far as the linear actuator is concerned) – depending only on power input from the drive.

 Technical data is used July 2003, safety factor taken into consideration S=1. Data applies for a temperature range of between -10°C and +40°C. The technical data applies under standard conditions and only for the individually specified operating mode and nature of load. In the case of compound loads, it must be verified in accordance with the laws of physics and technical standards, whether single data have to be reduced. Please contact us in the case of doubt.

## APPENDIX B: PRIME MOVER DATA

Catalog 8000-3/USA  
NeoMetric & J Series

### SERVO MOTORS

#### 92 mm, Encoder Feedback, Specifications

Parameter	Symbol	Units	N0921F	N0921G	N0922G	N0922J	N0923H	N0923K	N0924J	N0924K
Stall Torque Continuous <sup>1</sup>	$T_{cs}$	lb-in	15.5	15.6	27.6	28.3	41.3	40.6	54.6	54.8
		oz-in	249	249	442	453	660	650	873	876
		Nm	1.74	1.74	3.09	3.17	4.62	4.55	6.11	6.14
Stall Current Continuous <sup>1,4,8</sup>	$I_{cs}(\text{sine})$	Amps Peak	4.7	6.6	6.5	10.1	10.0	17.4	10.8	15.2
Stall Current Continuous <sup>1,7</sup>	$I_{cs}(\text{trap})$	Amps DC	4.1	5.7	5.6	8.7	8.6	15.1	9.4	13.2
Peak Torque <sup>6</sup>	$T_{pk}$	lb-in	46.6	46.7	82.9	83.5	123.7	121.9	163.8	164.3
		oz-in	746	747	1327	1336	1979	1951	2620	2629
		Nm	5.22	5.23	9.29	9.35	13.85	13.66	18.34	18.41
Peak Current <sup>4,8,9</sup>	$I_{pk}(\text{sine})$	Amps Peak	14.2	19.7	19.5	30.3	29.9	52.2	32.5	45.6
Peak Current <sup>7,9</sup>	$I_{pk}(\text{trap})$	Amps DC	12.3	17.1	26.9	26.2	25.9	45.2	28.2	39.5
Rated Speed <sup>2</sup>	$n_r$	rpm	6000	7500	4650	7300	4700	7500	3750	5250
Current @ Rated Speed	$I_r(\text{sine})$	Amps	4.1	5.2	5.6	7.0	8.6	11.9	9.7	12.4
Current @ Rated Speed	$I_r(\text{trap})$	Amps	3.5	4.5	4.8	6.0	7.4	10.3	8.4	10.7
Torque @ Rated Speed	$T_r$	lb-in	11.8	11.3	20.4	16.3	30.4	28.8	41.0	39.1
		oz-in	188	181	326	260	487	461	656	626
		Nm	1.32	1.27	2.28	1.82	3.41	3.23	4.59	4.38
Shaft Power @ Rated Speed	$P_{sh}$	watts	834	1004	1121	1404	1689	2557	1820	2431
Voltage Constant <sup>1,4</sup>	$K_v$	Volts/rad/s	0.427	0.309	0.556	0.360	0.540	0.305	0.627	0.470
Voltage Constant <sup>1,4</sup>	$K_v$	Volts/KRPM	44.72	32.36	59.22	37.70	56.55	31.94	68.80	49.22
Torque Constant <sup>9</sup>	$K_t(\text{sine})$	oz-in/Amp Peak	52.36	37.89	68.18	44.15	66.22	37.40	80.57	57.64
		Nm/Amp Peak	0.367	0.265	0.477	0.309	0.464	0.262	0.564	0.403
Torque Constant <sup>1,4</sup>	$K_t(\text{trap})$	oz-in/Amp DC	60.46	43.75	78.73	50.98	76.46	43.19	93.03	66.55
		Nm/Amp DC	0.423	0.306	0.551	0.357	0.535	0.302	0.651	0.466
Resistance <sup>3</sup>	$R$	Ohms	3.72	1.94	2.32	0.96	1.28	0.42	1.22	0.62
Inductance <sup>4</sup>	$L$	mH	17.11	8.99	14.72	6.18	14.95	4.78	20.60	10.51
Maximum Bus Voltage	$V_{bus}$	Volts DC	340	340	340	340	340	340	340	340
Thermal Res Wind-Amb	$R_{\theta JA}$	$^{\circ}\text{C}/\text{watt}$	1.06	1.06	0.91	0.91	0.7	0.7	0.62	0.62
Motor Constant	$K_{ms}$	oz-in/ $\sqrt{\text{watt}}$	31.35	31.41	51.69	52.03	67.59	66.64	84.23	84.52
		Nm/ $\sqrt{\text{watt}}$	0.219	0.220	0.362	0.364	0.473	0.466	0.590	0.592
Viscous Damping	$B$	oz-in/Krpm	0.5	0.5	0.8	0.8	1.1	1.1	1.4	1.4
		Nm/Krpm	3.5 E-3	3.5 E-3	5.6 E-3	5.6 E-3	7.7 E-3	7.7 E-3	9.8 E-3	9.8 E-3
Static Friction	$T_s$	oz-in	2.5	2.5	4.8	4.8	5.4	5.4	6.6	6.6
		Nm	1.8 E-2	1.8 E-2	3.4 E-2	3.4 E-2	3.8 E-2	3.8 E-2	4.6 E-2	4.6 E-2
Motor Thermal Time Constant	$\tau_{th}$	minutes	21.6	21.6	30	30	35	35	37	37
Electrical Time Constant	$\tau_{elec}$	milliseconds	4.60	4.63	6.34	6.44	11.68	11.38	16.89	16.95
NeoMetric Mech. Time Constant	$\tau_{mech}$	milliseconds	0.8	0.8	0.5	0.5	0.4	0.5	0.4	0.4
J Series Mech. Time Constant	$\tau_{mech}$	milliseconds	10.0	10.0	3.9	3.9	2.4	2.4	N/A	N/A
Intermittent Torque Duration <sup>10</sup>	$T_{int}$	seconds	48	48	39	39	61	61	61	61
Peak Torque Duration <sup>10</sup>	$T_{pk}$	seconds	17	17	13	13	16	16	15	15
NeoMetric Rotor Inertia	$J$	lb-in-sec <sup>2</sup>	3.6 E-4	3.6 E-4	6.2 E-4	6.2 E-4	8.8 E-4	8.8 E-4	1.1 E-3	1.1 E-3
		kg-m <sup>2</sup>	4.1 E-5	4.1 E-5	7.0 E-5	7.0 E-5	1.0 E-4	1.0 E-4	1.3 E-4	1.3 E-4
J Series Rotor Inertia	$J$	lb-in-sec <sup>2</sup>	4.2 E-3	4.2 E-3	4.5 E-3	4.5 E-3	4.8 E-3	4.8 E-3	N/A	N/A
		kg-m <sup>2</sup>	4.8 E-4	4.8 E-4	5.1 E-4	5.1 E-4	5.4 E-4	5.4 E-4	N/A	N/A
Number of Poles	$N_p$		4	4	4	4	4	4	4	4
NeoMetric Weight	#	lbs	8.1	8.1	11.7	11.7	15.1	15.1	18.0	18.0
		kg	3.7	3.7	5.3	5.3	6.9	6.9	8.2	8.2
J Series Weight	#	lbs	9.9	9.9	13.5	13.5	16.9	16.9	N/A	N/A
		kg	4.5	4.5	6.1	6.1	7.7	7.7	N/A	N/A
Winding Class			H	H	H	H	H	H	H	H

- 1 @ 25°C ambient, 125°C winding temperature, motor connected to a 10"x10"x1/4" aluminum mounting plate.
- 2 Maximum speed is 7500 RPM with 500 line Encoder. For 1000 line encoders, derate to 6000 RPM.
- 3 Measured Line to Line, +/- 10%.
- 4 Value is measured peak of sine wave.
- 5 +/- 30%, Line-to-Line, inductance bridge measurement @ 1KHz.
- 6 Initial winding temperature must be 60°C or less before Peak Current is Applied.

- 7 DC current through a pair of motor phases of a trapezoidally (six state) commutated motor.
- 8 Peak of the sinusoidal current in any phase for a sinusoidally commutated motor.
- 9 Total motor torque per peak of the sinusoidal amps measured in any phase, +/- 10%.
- 10 Maximum Time duration with 2 times rated current applied with initial winding temp at 60°C.
- 11 Maximum Time duration with 3 times rated current applied with initial winding temp at 60°C.

Note: These specifications are based on theoretical motor performance and are not specific to any amplifier.

THIS PAGE INTENTIONALLY LEFT BLANK



## APPENDIX C: CONTROLLER DATA

Catalog 8000-4/USA  
6K Controllers

### 6K CONTROLLERS

Specifications		
Parameter	Parameter Type	Value
Power	Input	24 VDC, 2 Amp, User Supplied Additional power may be required for I/O use See Installation Guide for Details
Environmental	Operating Temperature	32° to 122°F (0° to 50°C)
	Storage Temperature	-22° to 185°F (-30° to 85°C)
	Humidity	0% to 95% non-condensing
Performance	Command	+/- 10V or Step & Direction Configurable per axis
	Servo Update	As fast as 62.5 µs/axis
	Encoder	Two phase quadrature detect incremental encoders with differential (recommended) or single ended outputs (+5 VDC TTL compatible) Max Frequency = 12 MHz post quadrature
	Stepping Accuracy	+/-0 steps from preset total
	Position Range	+/-2,147,483,648 counts
	Velocity Range	1 to 2,048,000 counts/sec (step & direction output) 1 to 12,000,000 counts/sec (+/- 10V output)
	End-of-Travel & Home Limits per axis	Factory default is 24 VDC sourcing Jumper LIM-P to GND for sinking 0-24 VDC range through VIN <sub>ref</sub> 1/3 1/3 1/3 voltage switching threshold Configurable as programmable inputs if not needed as limits
Inputs	Onboard	Fast trigger inputs 9 on 6K2 & 6K4, 17 on 6K6 & 6K8 Factory default is 24 VDC sourcing Jumper TRIG-P to GND for sinking 0-24 VDC range through VIN <sub>ref</sub> 1/3 1/3 1/3 voltage switching threshold
	EVM32 Expansion (optional)	Up to 256 digital inputs (2 ms update rate) Up to 64 12-bit analog inputs (+/- 10 VDC) 12-24 VDC user supplied through EVM32 module 1/3 1/3 1/3 voltage switching threshold on digital inputs LEDs provided on digital inputs for visual reference
	Outputs	Onboard 5-24 VDC user supplied 300 mA maximum current sink 4 on 6K2 & 6K4, 8 on 6K6 & 6K8
Communications	Ethernet	10 Base-T (10Mbps Twisted Pair) Multiple protocols
	Serial	RS-232, RS-485 2-wire or 4-wire Up to 115,200 baud, Up to 99 units in daisy-chain or multi-drop
	* Maximum number of outputs and maximum current sink are heat dependent. See product documentation for duty cycle considerations.	

Discover How The 6K Motion Controller Can Solve Your Next Application. Call 1-800-358-9070 Today.

THIS PAGE INTENTIONALLY LEFT BLANK

## APPENDIX D: VIDEO CAMERA DATA



### WAT-902H 2 / 3 ULTIMATE

#### SPECIFICATIONS

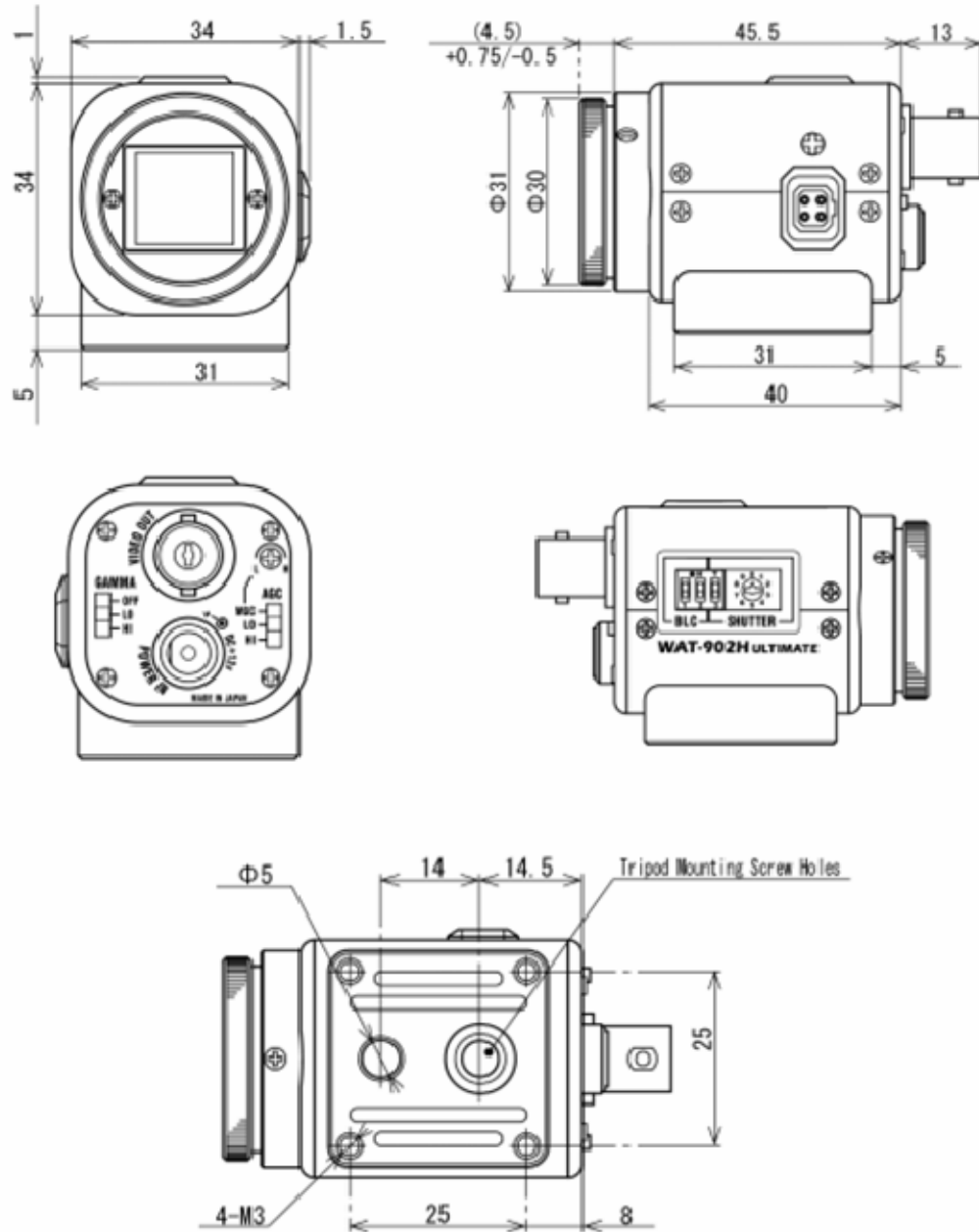
Model	WAT-902H2 ULTIMATE (EIA)	WAT-902H2 ULTIMATE (CCIR)
Pick-up element	1/2" interline transfer CCD image sensor	
Number of total pixels	811(H) × 508(V)	795(H) × 596(V)
Number of effective pixels	768(H) × 494(V)	752(H) × 582(V)
Unit cell size	8.4μm (H) × 9.8μm (V)	8.6μm (H) × 8.3μm (V)
Shutter speeds	EI1: 1/60 sec. - 1/100000 sec. EI2: 1/100 sec. - 1/100000 sec. FL: 1/100 sec. OFF: 1/60 sec.	EI1: 1/50 sec. - 1/100000 sec. EI2: 1/120 sec. - 1/100000 sec. FL: 1/120 sec. FL: 1/50 sec.
	1/250, 1/500, 1/1000, 1/2000, 1/5000, 1/10000, 1/100000 sec.	
Minimum illumination	0.0001 lx, F1.4	

Model	WAT-902H3 ULTIMATE (EIA)	WAT-902H3 ULTIMATE (CCIR)
Pick-up element	1/3" interline transfer CCD image sensor	
Number of total pixels	811(H) × 508(V)	795(H) × 596(V)
Number of effective pixels	768(H) × 494(V)	752(H) × 582(V)
Unit cell size	6.35μm (H) × 7.40μm (V)	6.50μm (H) × 6.25μm (V)
Shutter speeds	EI1: 1/60 sec. - 1/100000 sec. EI2: 1/100 sec. - 1/100000 sec. FL: 1/100 sec. OFF: 1/60 sec.	EI: 1/50 sec. - 1/100,000 sec. EI2: 1/120 sec. - 1/100000 sec. FL: 1/120 sec. FL: 1/50 sec.
	1/250, 1/500, 1/1000, 1/2000, 1/5000, 1/10000, 1/100000 sec.	
Minimum illumination	0.0002 lx, F1.4	

Common specifications	
Synchronizing system	Internal sync.
Video output	1Vp-p, 75ohms, unbalanced
Resolution (H)	570TVL (Center)
SN ratio	More than 50dB (AGC OFF)
AGC	①HI: 5-60dB ②LO: 5-32dB ③MGC(5-60dB)
Back light compensation	①OFF(Default) ②Center ③Lower ④Center + lower
Gamma correction	①HI (γ≒0.35) ②LO (γ≒0.45) ③OFF (γ≒1)
Power supply	DC12V±10%
Power consumption	1.32W (110mA)
Operating temperature	-10°C - +40°C
Storage temperature	-30°C - +70°C
Dimensions(W×H×L)	35.5 × 40 × 63 (mm)
Weight	approx. 98g

Design and specifications are subject to change without notice.

# **DIMENSIONS (mm)**





## APPENDIX E: MOTOR TRANSFER FUNCTION DATA

Motion Direction	Elevation Up	Elevation Down	Azimuth Back	Azimuth Forward
$k_m$	0.0127	0.0136	0.0155	0.0153
$\tau_m$	0.0904	0.0710	0.0728	0.0772
$\frac{\omega(s)}{V_{in}}$	$\frac{0.0127}{0.09s + 1}$	$\frac{0.0136}{0.071s + 1}$	$\frac{0.0155}{0.0728s + 1}$	$\frac{0.0153}{0.0772s + 1}$
$\frac{\theta(s)}{V_{in}}$	$\frac{0.0127}{s(0.09s + 1)}$	$\frac{0.0136}{s(0.071s + 1)}$	$\frac{0.0155}{s(0.0728s + 1)}$	$\frac{0.0153}{s(0.0772s + 1)}$

THIS PAGE INTENTIONALLY LEFT BLANK

## APPENDIX F: MATLAB CODE FOR DETERMINING THE MOTOR TRANSFER FUNCTIONS

```
%*****
% Motor Measurements.m - Measures & plots motor position and
%                          angular velocities of each axis.
%
% LCDR Scott Johnson, Jan 06
%*****

%%
%*****
****
%                               Elevation Up Measurements
%*****
****

%close all
%clear all
clc

%*** Prep axis for test ***

HomePosition;% Send the Source to the home position.
pause(1);
BAO_Motion2(0,5, 0,0);pause(8.0);BAO_Motion2(0,0, 0,0); % bring source
all the way down
pause(2)

%*** Initialization ***

% 5V=6.5s

voltage = 10; % motor voltage for test
t = 3.5; % period of test in seconds

t = t/0.01; % segment test period time segments to be used in arrays.
See for loop below

Time = zeros(1,t); % time array
read = zeros(1,t); % encoder reading array

encoders = BAO_Motion2(0,0, 0,0); %take initial reading
read(1) = encoders(4); % read encoder count
Time(1) = 0; % initial time is zero

%*** Start Test ***

BAO_Motion2(0,-voltage, 0,0); tic %start motion & time
```

```

for i=1:t; % carry out readings for t*0.01 seconds; period=pause*i(max)
    encoders = BAO_Motion2(0,-voltage, 0,0); % read encoders
    Time(i+1) = toc; % read time
    read(i+1) = encoders(4); % choose elevation encoder reading
(counts)
    pause(0.01)
end

BAO_Motion2(0,0, 0,0); % Stop motion

***** Calculations *****

dX=diff(read);
dT=diff(Time);

vel = dX./dT; % velocity in counts/s

w = vel.*(1/57296); % angular velocity. 1 rad = 57296 counts

***** Plots *****

% First need to calc time interval midpoint for each angular vel

for i = 1:t
    w_time(i) = Time(i+1) - dT(i)/2;
end

% plot time vs angular vel (rads/sec)

plot(w_time,w)
xlabel('time (sec)')
ylabel('Angular Velocity (rads/sec)')
title(['Elevation Up Instantaneous Angular Velocity (rads/s) for',
Voltage = ',num2str(voltage),' V'])
grid
%
%
% % plot calculated velocity response curve
%
% Km=0.012
% a=10
% Tm=0.057
% Wt=Km*a*(1-exp(-w_time/Tm))
% hold
% plot(w_time,Wt)
% Wt2=Km*a*(1-exp(-Time/Tm))
% plot(Time,Wt2,'c')

% plot time vs angular vel (degrees/sec)

% figure
% plot(w_time,w.*(180/pi))

```

```

% xlabel('time (sec)')
% ylabel('Angular Velocity (degrees/sec)')
% title(['Elevation Up Instantaneous Angular Velocity (deg/s) for
Voltage = ',num2str(voltage),' V'])
% grid

% plot time vs position (rads)

% figure
% plot(Time,read./57296)
% xlabel('time (sec)')
% ylabel('Position (rads)')
% title(['Elevation Up Position (rads)for Voltage =
',num2str(voltage),' V'])
% grid

% Plot calculated position response curve and velocity.  Need to use
simulink file
% elevation_up.mdl

hold
% plot(sim_time,-0.18+Position,'r')
plot(sim_time,velocity,'r')
legend('Measured Data','Transfer Function')

% plot time vs position (degrees)

% figure
% plot(Time,(read./57296)*180/pi)
% xlabel('time (sec)')
% ylabel('Position (degrees)')
% title('Elevation Up Position (degrees)for Voltage =
',num2str(voltage),' V'])
% grid

%%

%*****
****
%%
Elevation Down Measurements
%*****
****

%clear all
clc

%*** Prep axis for test ****

HomePosition;% Send the Source to the home position.
pause(1);
BAO_Motion2(0,-5, 0,0);pause(4.2);BAO_Motion2(0,0, 0,0); % bring source
all the way up
pause(2)

```

```

%*** Initialization ***

% 5V = 5sec

voltage = 10 % motor voltage for test
t = 3.0 % period of test in seconds

t = t/0.01 % segment test period time segments to be used in arrays.
See for loop below

Time = zeros(1,t); % time array
read = zeros(1,t); % encoder reading array

encoders = BAO_Motion2(0,0, 0,0); %take initial reading
read(1) = encoders(4); % read encoder count
Time(1) = 0; % initial time is zero

%*** Start Test ***

BAO_Motion2(0,voltage, 0,0); tic %start motion & time

for i=1:t; % carry out readings for t*0.01 seconds; period=pause*i(max)
    encoders = BAO_Motion2(0,voltage, 0,0); % read encoders
    Time(i+1) = toc; % read time
    read(i+1) = encoders(4); % choose elevation encoder reading
    pause(0.01)
end

BAO_Motion2(0,0, 0,0); % Stop motion

%***** Calculations *****

dX = zeros(1,t); % initialization
dT = zeros(1,t); % initialization

for i=1:t % calculate dX & dT
    dX(i) = read(i+1) - read(i);
    dT(i) = Time(i+1) - Time(i);
end

vel = dX./dT; % velocity in counts/s

w = vel.*(1/57296); % angular velocity. 1 rad = 57296 counts

%***** Plots *****

% First need to calc time interval midpoint for each angular vel

for i = 1:t
    w_time(i) = Time(i+1) - dT(i)/2;
end

```

```

% plot time vs angular vel (rads/sec)

figure
plot(w_time,-w)
xlabel('time (sec)')
ylabel('Angular Velocity (rads/sec)')
title(['Elevation Down Instantaneous Angular Velocity (rads/s) for Voltage = ',num2str(voltage),' V'])
grid

% Plot Transfer function. Must run Simulink Model elevation_down.mdl first to get sim_time &
% velocity
hold
plot(sim_time,velocity,'r')
legend('Measured Data','Transfer Function')

%
% % plot calculated response curve
%
% Km=0.0093
% a=10
% Tm=0.112
% Wt=Km*a*(1-exp(-w_time/Tm))
% hold
% plot(w_time,Wt,'r')

% plot time vs angular vel (degrees/sec)

% figure
% plot(w_time,w*(180/pi))
% xlabel('time (sec)')
% ylabel('Angular Velocity (degrees/sec)')
% title(['Elevation Down Instantaneous Angular Velocity (deg/s)for Voltage = ',num2str(voltage),' V'])
% grid

% plot time vs position (rads)

% figure
% plot(Time,read./57296)
% xlabel('time (sec)')
% ylabel('Position (rads)')
% title(['Elevation Down Position (rads) for Voltage = ',num2str(voltage),' V'])
% grid

% plot time vs position (degrees)

% figure
% plot(Time,(read./57296)*180/pi)

```

```

% xlabel('time (sec)')
% ylabel('Position (degrees)')
% title(['Elevation Down Position (degrees) for Voltage = ',num2str(voltage),' V'])
% grid
%%

%*****
****
%%                               Azimuth Back Measurements
%*****
****

%clear all
clc

%*** Prep axis for test ***

HomePosition;% Send the Source to the home position.
pause(1);
BAO_Motion2(-5,0, 0,0);pause(5.0);BAO_Motion2(0,0, 0,0); % bring source
all the way fwd
pause(2)

%*** Initialization ***

voltage = 10; % motor voltage for test
t = 2.5; % period of test in seconds

t = t/0.01; % segment test period time segments to be used in arrays.
See for loop below

Time = zeros(1,t); % time array
read = zeros(1,t); % encoder reading array

encoders = BAO_Motion2(0,0, 0,0); %take initial reading
read(1) = encoders(3); % read encoder count
Time(1) = 0; % initial time is zero

%*** Start Test ***

BAO_Motion2(voltage,0, 0,0); tic %start motion & time

for i=1:t; % carry out readings for t*0.01 seconds; period=pause*i(max)
    encoders = BAO_Motion2(voltage,0, 0,0); % read encoders
    Time(i+1) = toc; % read time
    read(i+1) = encoders(3); % choose azimuth encoder reading
    pause(0.01)
end

BAO_Motion2(0,0, 0,0); % Stop motion

%***** Calculations *****

```



```

dX = zeros(1,t); % initialization
dT = zeros(1,t); % initialization

for i=1:t % calculate dX & dT
    dX(i) = read(i+1) - read(i);
    dT(i) = Time(i+1) - Time(i);
end

vel = dX./dT; % velocity in counts/s

w = vel.*(1/57296); % angular velocity. 1 rad = 57296 counts

%***** Plots *****

% First need to calc time interval midpoint for each angular vel

for i = 1:t
    w_time(i) = Time(i+1) - dT(i)/2;
end

% plot time vs angular vel (rads/sec)

figure
plot(w_time,abs(w))
xlabel('time (sec)')
ylabel('Angular Velocity (rads/sec)')
title(['Azimuth Back Instantaneous Angular Velocity (rads/s) for',
Voltage = ',num2str(voltage), ' V'])
grid

% Plot Transfer function. Must run Simulink Model Azimuth_back.mdl
first to get sim_time &
% velocity

hold
plot(sim_time,velocity,'r')
legend('Measured Data','Transfer Function')

% plot calculated response curve

% Km=0.0155
% a=10
% Tm=0.048
% Wt=Km*a*(1-exp(-w_time/Tm))
% hold
% plot(w_time,Wt,'r')

% plot time vs angular vel (degrees/sec)

% figure
% plot(w_time,abs(w*(180/pi)))
% xlabel('time (sec)')

```

```

% ylabel('Angular Velocity (degrees/sec)')
% title(['Azimuth Back Instantaneous Angular Velocity (deg/s) for
Voltage = ',num2str(voltage),' V'])
% grid

% plot time vs position (rads)

% figure
% plot(Time,read./57296)
% xlabel('time (sec)')
% ylabel('Position (rads)')
% title(['Azimuth Back Position (rads) for Voltage =
',num2str(voltage),' V'])
% grid

% plot time vs position (degrees)

% figure
% plot(Time,(read./57296)*180/pi)
% xlabel('time (sec)')
% ylabel('Position (degrees)')
% title(['Azimuth Back Position (degrees)for Voltage =
',num2str(voltage),' V'])
% grid

%%

*****
****
%%
Azimuth Fwd Measurements
*****

%clear all
clc

**** Prep axis for test ****

HomePosition;% Send the Source to the home position.
pause(1);
BAO_Motion2(5,0, 0,0);pause(6.0);BAO_Motion2(0,0, 0,0); % bring source
all the way fwd
pause(2)

**** Initialization ****

voltage = 10; % motor voltage for test
t = 2.5; % period of test in seconds

t = t/0.01; % segment test period time segments to be used in arrays.
See for loop below

Time = zeros(1,t); % time array
read = zeros(1,t); % encoder reading array

```

```

encoders = BAO_Motion2(0,0, 0,0); %take initial reading
read(1) = encoders(3); % read encoder count
Time(1) = 0; % initial time is zero

%*** Start Test ***

BAO_Motion2(-voltage,0, 0,0); tic %start motion & time

for i=1:t; % carry out readings for 8 seconds; period=pause*i(max)
    encoders = BAO_Motion2(-voltage,0, 0,0); % read encoders
    Time(i+1) = toc; % read time
    read(i+1) = encoders(3); % choose elevation encoder reading
    pause(0.01)
end

BAO_Motion2(0,0, 0,0); % Stop motion

%***** Calculations *****

dX = zeros(1,t); % initialization
dT = zeros(1,t); % initialization

for i=1:t % calculate dX & dT
    dX(i) = read(i+1) - read(i);
    dT(i) = Time(i+1) - Time(i);
end

vel = dX./dT; % velocity in counts/s

w = vel.*(1/57296); % angular velocity. 1 rad = 57296 counts

%***** Plots *****

% First need to calc time interval midpoint for each angular vel

for i = 1:t
    w_time(i) = Time(i+1) - dT(i)/2;
end

% plot time vs angular vel (rads/sec)

figure
plot(w_time,w)
xlabel('time (sec)')
ylabel('Angular Velocity (rads/sec)')
title(['Azimuth Fwd Instantaneous Angular Velocity (rads/s) for Voltage'
= ',num2str(voltage),' V'])
grid

```

```

% Plot Transfer function.  Must run Simulink Model Azimuth_fwd.mdl
first to get sim_time &
% velocity

hold
plot(sim_time,velocity,'r')
legend('Measured Data','Transfer Function')

% plot calculated response curve

% Km=0.0147
% a=10
% Tm=0.04
% Wt=Km*a*(1-exp(-w_time/Tm))
% hold
% plot(w_time,Wt,'r')

% plot time vs angular vel (degrees/sec)

% figure
% plot(w_time,w*(180/pi))
% xlabel('time (sec)')
% ylabel('Angular Velocity (degrees/sec)')
% title(['Azimuth Fwd Instantaneous Angular Velocity (deg/s) for
Voltage = ',num2str(voltage),' V'])
% grid

% plot time vs position (rads)

% figure
% plot(Time,read./57296)
% xlabel('time (sec)')
% ylabel('Position (rads)')
% title(['Azimuth Fwd Position (rads)for Voltage = ',num2str(voltage),'
V'])
% grid

% plot time vs position (degrees)

% figure
% plot(Time,(read./57296)*180/pi)
% xlabel('time (sec)')
% ylabel('Position (degrees)')
% title(['Azimuth Fwd Position (degrees) for Voltage =
',num2str(voltage),' V'])
% grid

%%

HomePosition; % end of Test

```

## APPENDIX G: MATLAB CODE FOR FSM EXPERIMENTAL TESTING

```
%*****
% FSM_transfer_function.m - Drives FSM for TF testing
%
% LCDR Scott Johnson, Jul 06
%*****

%%
% Calibration
pause(5)
BAO_Motion2(0,0,-0.50,0);pause(0.000001);BAO_Motion2(0,0, 0,0);
%%

% Draw a circle

BAO_Motion2(1000000,0, 0,0);
for x=0:0.1:10
BAO_Motion2(0,0,sin(x),cos(x));
pause(0.1)
end
BAO_Motion2(0,0, 0,0);
BAO_Motion2(-1000000,0, 0,0);

%%
% ** Chirp test **

% y = chirp(t,f0,t1,f1) generates samples of a linear swept-frequency
cosine signal at the time
% instances defined in array t, where f0 is the instantaneous frequency
at time 0, and f1 is
% the instantaneous frequency at time t1. f0 and f1 are both in hertz.
% If unspecified, f0 is 0, t1 is 1, and f1 is 100.
%%
clear all

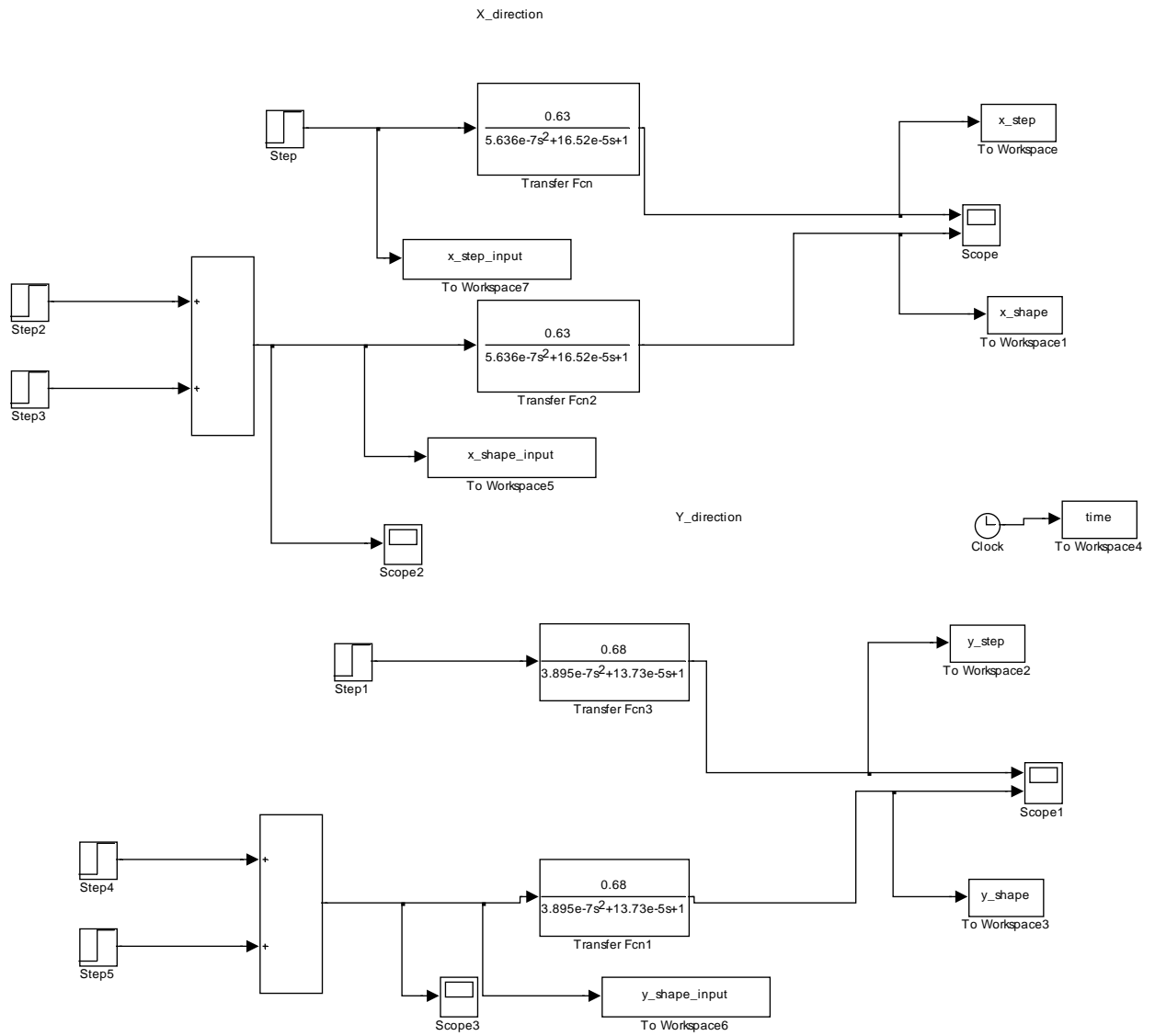
BAO_Motion2(1000000,0, 0,0);
END = 100; %33 = 34 sec
count = 0;
end_freq = 1000;
interval = 0.000037;

t=0:interval:END;
y = chirp(t,0,END,end_freq);

count = 0;
%%
tic
for t1=0:interval:END
```

```
count = count+1;  
V = 0.3*y(count);  
BAO_Motion2(0,0,V,0); %(x,x,y-dir,x-dir)  
end  
toc  
BAO_Motion2(0,0, 0,0);  
BAO_Motion2(-1000000,0, 0,0);
```

## APPENDIX H: SIMULINK MODEL OF FAST STEERING MIRROR



THIS PAGE INTENTIONALLY LEFT BLANK



## APPENDIX I: MATLAB CODE FOR MOTOR AND FAST STEERING MIRROR CONTROL

```
%*****
%TrackNPS_Beacons.m
% Created by Baker Adaptive Optics
%
% Modified by: Scott Johnson
%*****

% Note: Sticktion voltage on azimuth axis = 2.7 volts
%       Sticktion voltage on elevation axis = 3.6 volts

% Note: TASS2 must be level before starting the test.
%*****
****
%                               Initializations
%*****
****
%%
close all;clear all;clc

% *** Start initializing the platform *****

monograb(2); % deinitialize frame-grabber camera
clear -mex;

Set_Iterations = 1200; % Set the number of iterations the tracking
sequence will run.
                        % Approx 30 secs per 1000 interations.

iteration = 0;

dX_previous = 0;

HomePosition; % Send the Source to the home position. This also
initializes the mount controller.
pause(1);
% end track
BAO_Motion2(0,5, 0,0);pause(3.8);BAO_Motion2(0,0, 0,0); %pre-set the
elevation to look near the 3 spots
BAO_Motion2(-5,0, 0,0);pause(0.25);BAO_Motion2(0,0, 0,0); %pre-set the
azimuth to look near the 3 spots
% middle track
% BAO_Motion2(0,5, 0,0);pause(3.1);BAO_Motion2(0,0, 0,0);
% BAO_Motion2(5,0, 0,0);pause(1.5);BAO_Motion2(0,0, 0,0);

% % Jeffs Platform
% BAO_Motion2(0,5, 0,0);pause(4.7);BAO_Motion2(0,0, 0,0);
% BAO_Motion2(-5,0, 0,0);pause(1.5);BAO_Motion2(0,0, 0,0);

pause(2);
```

```

monograb(0);monograb(1); % Initialize frame-grabber

BW=monograb(1);

image(BW');colormap Gray(255);axis
image;set(gcf,'backingstore','off','doublebuffer','on');pause(1);

Pixel_Test % Call this program to get telescope offsets in pixels
%%
%*****
%Calcs for FSM Input Shaping
%*****
wx = 2*pi*212;
Td_x = 4.8e-3;
zeta_x = 0.11;
Kx = exp((-zeta_x)/sqrt(1-zeta_x^2));
Ax_1 = 1/(1+Kx);
Ax_2 = Kx/(1+Kx);

wy = 2*pi*251;
Td_y = 3.9e-3;
zeta_y = 0.11;
Ky = exp((-zeta_y)/sqrt(1-zeta_y^2));
Ay_1 = 1/(1+Kx);
Ay_2 = Kx/(1+Kx);

%%
to = clock; % initialization to calculate running time. See cmd
>>etime at end of program
tic;told=0;

%*****
***
%
% Begin Iteration Loop
%*****
****

%*****
% Locate and mark beacons
%*****

    for i=1:Set_Iterations; %set how many iterations the tracking
sequence will run
        iteration = iteration+1;
        BW=monograb(1);%First, Grab an image
        Xc(1)=0;Xc(2)=0;Xc(3)=0;Yc(1)=0;Yc(2)=0;Yc(3)=0;%then, zero out the
3 spot x,y coordinates
        %Now, your task is to locate the 3 beacon spots.
        for m=1:3; %perform the search 3 times, so that you can find
them all
            %"Cheap" Centroiding finds the first brightest spot
            [Vbw,Ybw]=max(max(BW));
            [Vbw,Xbw]=max(BW(:,Ybw));
            s=15;%boxsize=s*2+1, s=kind of box radius

```

```

        if (Xbw<s+1)|(Xbw>640-s-1)|(Ybw<s+1)|(Ybw>480-s-1); %if a
spot is too close to the edge,
            Vbw=0; %then
set it's brightness to zero
        end;

        %"Inexpensive" Centroiding starts with "Cheap" Result
        if Vbw >50 %if the spot
was brightest spot was bright enough

            Box=double( BW(Xbw-s:Xbw+s,Ybw-s:Ybw+s) ); %Then grab the
box with the spot in it
            for j=1:2*s+1 %loop over the
box
                for k=1:2*s+1 %loop over the
box
                    if Box(j,k)<25 %threshold the
data at 25 counts
                        Box(j,k)=0;
                    else
                        %BW(Xbw-s+j-1,Ybw-s+k-1)=0; %black-out the
>25 ct spots in the original image
                    end; % (you can see
some parts of the spots in the image graphics)
                        BW(Xbw-s+j-1,Ybw-s+k-1)=0; %black-out the
entire box in the original image
                    end;
                end;
            [X,Y]=meshgrid(Xbw-s:Xbw+s,Ybw-s:Ybw+s); %define the
pixels in original image space for the box
            Sum=sum(sum(Box)); %compute the
sum of the box for the centroid calc.
            Xc(m)=sum(sum(X.*Box'))/(Sum+.0000001); %compute the X
centroid of this iteration
            Yc(m)=sum(sum(Y.*Box'))/(Sum+.0000001); %compute the Y
centroid of this iteration
        end;
    end; %now go on to
the next bright spot

    %At this stage, you have located three centroids of the three
brightest
    %spots in the image BW.

    d(1)=sqrt( (Xc(2)-Xc(1))^2 + (Yc(2)-Yc(1))^2 ); %compute the
distance between spots 1 and 2
    d(2)=sqrt( (Xc(2)-Xc(3))^2 + (Yc(2)-Yc(3))^2 ); %compute the
distance between spots 2 and 3
    d(3)=sqrt( (Xc(1)-Xc(3))^2 + (Yc(1)-Yc(3))^2 ); %compute the
distance between spots 1 and 3

    %Next we determine which of the points 1,2, and 3 are A,B, and C

    [longest,ilongest]=max(d); %B-C
    [shortest,ishortest]=min(d); %A-B
    if ( (ilongest==2)&(ishortest==1) )

```

```

        A=1;B=2;C=3;
    elseif( (ilongest==3)&(ishortest==1) )
        A=2;B=1;C=3;
    elseif( (ilongest==1)&(ishortest==2) )
        A=3;B=2;C=1;
    elseif( (ilongest==3)&(ishortest==2) )
        A=2;B=3;C=1;
    elseif( (ilongest==2)&(ishortest==3) )
        A=1;B=3;C=2;
    elseif( (ilongest==1)&(ishortest==3) )
        A=3;B=1;C=2;
    end;

    %Now we know which spots are which:
    %      ( Xc(A),Yc(A) ) are the coords of spot A
    %      ( Xc(B),Yc(B) ) are the coords of spot B
    %      ( Xc(C),Yc(C) ) are the coords of spot C

    % **** Account for rotation of Beacons ***

    TASS_Rotation = asind((Yc(B)-Yc(A))/Hyp_Tele); % degrees

    Xa_R = Xc(B)+(Xc(A)-Xc(B))*cosd(TASS_Rotation);
    Ya_R = Yc(A)-(Xc(A)-Xc(B))*cosd(TASS_Rotation)*tand(TASS_Rotation);
    X_Tele_R = Xa_R+Hyp_Tele*cosd(TASS_Rotation+Ang_Tele);
    Y_Tele_R = Ya_R-Hyp_Tele*sind(TASS_Rotation+Ang_Tele);

    Xsrc=430;Ysrc=180; % This is the location of the source.
                      % Measured in pixels from the top left of camera
display.

                      % Need to fine tune this parameter by statically
                      % running source motors. On target = 430,170

    %check to see if the distance around the spots is reasonable to see
    if
        %all 3 are measured properly and realistic. The sum should be
        around
        %125. If the spots are not likely to be real, call the error zero
        and
        %stop moving until they come back.
        % if (sum(d)>150)|(sum(d)<100); Xtele=Xoff;Ytele=Yoff; end
        % if iteration==Set_Iterations
        % imageesc(BW');axis image;hold on;text(Xc(A),Yc(A),'A','Color','w');
        %
        text(Xc(B),Yc(B),'B','Color','w');
        %
        text(Xc(C),Yc(C),'C','Color','w');
        %
        text(X_Tele_R,Y_Tele_R,'T','Color','b');
        %
        % text(Xsrc,Ysrc,'S','Color','r');
        % hold off;drawnow;
    end

```

```

dX=Xsrc-X_Tele_R;    %compute the error in X (azimuth)
dY=Ysrc-Y_Tele_R;    %compute the error in Y (elevation)

%*****
%                               Control Actions
%*****

%*****
% Motor Controls
%*****

%*****      P Gain      *****

    Vaz=dX/(-13); %minus sign account for directional difference dX and
intended direction
    Vel=dY/(-25); %minus sign account for directional difference dX and
intended direction

% ***** Integral Calcs *****
% start on 20th iteration

if i>50
    Area = dX+dX_previous;
    dX_previous = Area;
    Vaz=Vaz+0.0000001*abs(Area);
end

%***** Correct Voltages for Dynamic Friction
*****

%    if Vaz<0;Vaz=Vaz-1.7;end;if Vaz>0;Vaz=Vaz+1.9;end;
    if Vaz<0;Vaz=Vaz-2;end;if Vaz>0;Vaz=Vaz+2;end;
    if Vel<0;Vel=(Vel-4);end;if Vel>0;Vel=(Vel+4);end;

%***** Set limits on Voltages +- 10V
*****

    if Vaz>10.;Vaz=10;end;if Vaz<-10;Vaz=-10;end;%define upper and
lower limits for drive voltage azimuth
    if Vel>10.;Vel=10;end;if Vel<-10;Vel=-10;end;%define upper and
lower limits for drive voltage elevation

%***** Initial Voltage
*****

%Set initial voltage to 3 volts on first iteration to overcome
static
%friction (sticktion)

if iteration==1
    if Vaz<0;Vaz=-3;end;if Vaz>0;Vaz=3;end;
    if Vel<0;Vel=-4;end;if Vel>0;Vel=4;end;

```

```

end

%***** Deadzone *****
% Create a Deadzone for motors to stop working

if abs(dX) < (0.9*15*X_Pix_ratio); % [max mirror movement (15mm)]
* X_Pix_ratio(pixels/mm) = max FSM movement (pixels)
    Vaz=0;
    dX_previous = 0;
end

if abs(dY)< (0.9*15*Y_Pix_ratio); % [max mirror movement (15mm)]
* Y_Pix_ratio(pixels/mm) = max FSM movement (pixels)
    Vel=0;
end

%%
%*****
% Fast Steering Mirror Commands.
%*****

% ***** Conversions *****
% Convert dx and dy into voltages. Tests showed that when the
% mirror is given 0.6V the movement is approx 15mm at TASS2

Vx = (dX/X_Pix_ratio)*(0.6/15);
%(dX(pix)/X_pix_ratio(pix/mm))*(0.6V/15mm)=Volts
Vy = (dY/Y_Pix_ratio)*(0.6/15);
%(dY(pix)/Y_pix_ratio(pix/mm))*(0.6V/15mm)=Volts

%***** Set Maximum Voltages *****
% set maximum FSM voltage at 0.6 volts
% voltages greater than 0.6V drives the laser out of the optics
range

if Vx > 0.6; Vx = 0.6;end
if Vx < -0.6; Vx = -0.6;end

if Vy > 0.6; Vy = 0.6; end
if Vy < -0.6; Vy = -0.6; end

Mx=Vx*15/0.6*X_Pix_ratio; % mirror movement in x-direction
(pixels)
% Vx(volts)*(15mm/0.6volts)*(pix/mm)
My=Vy*15/0.6*Y_Pix_ratio; % mirror movement in y-direction
(pixels)

Xmirror = Xsrc-Mx;
Ymirror = Ysrc-My;

Virtual_dX = Xmirror - X_Tele_R; % Difference btw Telescope and
laser w/mirror movement
Virtual_dY = Ymirror - Y_Tele_R;

```

```

%*****Change polarity on voltages to match mirror directions***

% Note: this matrix takes into account the mirror voltage
directions
%       as well as the error directions fm the image.

V = [1 0;0 -1]*[Vy;Vx]; % Scott
%V = [0 -1;-1 0]*[Vx;Vy]; % Jae
Vxx = V(1);
Vyy = V(2);

%%
%***** Movement Commands w/Input
Shaping*****

BAO_Motion2(Vaz,Vel,Ax_1*Vxx,Ay_1*Vyy);
pause(Td_y/2)
BAO_Motion2(Vaz,Vel,Ax_1*Vxx,Vyy);
pause(Td_x/2-Td_y/2)
BAO_Motion2(Vaz,Vel,Vxx,Vyy);

% BAO_Motion2(Vaz,Vel,0,0);

% BAO_Motion2(0,0,Ax_1*Vxx,Ay_1*Vyy);
% pause(Td_y/wy)
% BAO_Motion2(0,0,Ax_1*Vxx,Vyy);
% pause(Td_x/wx-Td_y/wy)
% BAO_Motion2(0,0,Vxx,Vyy);

tnew=toc;
dt = tnew-told;
freq=1/(dt);
told=toc;

%***** Create arrays for plots
*****

X_error(iteration)= dX;
Y_error(iteration)= dY;
V_azimuth(iteration) = Vaz;
V_elevation(iteration) = Vel;
V_x(iteration) = Vxx;
V_y(iteration) = Vyy;
frequency(iteration)= freq;
Time(iteration) = toc;
%AREA(iteration)=Area;
D1_2(iteration) = d(1);
D2_3(iteration) = d(2);
D3_1(iteration) = d(3);
XA(iteration) = Xc(A);
YA(iteration)= Yc(A);
XB(iteration) = Xc(B);
YB(iteration)= Yc(B);

```

```

    Virtual_x(iteration) = Virtual_dX;
    Virtual_y(iteration) = Virtual_dY;
    M_x(iteration) = Mx;
    X_mirror(iteration) = Xmirror;
    M_y(iteration) = My;

end; % end of iteration loop

total_time = etime(clock,to);
BAO_Motion2(0,0, 0,0);%stop the motors when you're done!
monograb(2); % de-initialize the camera

%*****
%                               Post Operation Procedures
%*****

%***** Display Performance Stats in workspace *****
results=[X_error;Y_error;V_x;V_y];
results = [Xc(A) Yc(A);Xc(B) Yc(B); Yc(A)-Yc(B) 0]

% plot(Time,V_x,Time,V_y,'--')
% legend('Vx','Vy')
%
% figure
% plot(Time,V_azimuth,Time,V_elevation,'--')
% legend('Vaz','Velev')
% total_time

avg_freq = mean(frequency)

%*****
% Create Error Plots
%*****
%%
% Plot X_error & Azimuth Voltage

[AX,H1,H2]= plotyy(Time,X_error,Time,V_azimuth)
title('X Error Plot')
xlabel('Time (sec)')
ylabel('X Error (pixels)')
set(get(AX(2),'Ylabel'),'String','Azimuth Voltage (V)')
set(H2,'LineStyle','--')
grid
axis

figure
hold on
plot(Time,V_azimuth)
plot(Time,X_error,'r')
axis([0 30 -15 5])
title('X Error Plot')
plot(Time,Virtual_x,'g')
grid
legend('Az Volts','X_error','Virtual Error')

```



```

% Plot Y_error & Elevation Voltage

figure
[AX,H1,H2]= plotyy(Time,Y_error,Time,V_elevation)
title('Y Error Plot')
xlabel('Time (sec)')
ylabel('Y Error (pixels)')
set(get(AX(2),'Ylabel'),'String','Elevation Voltage (V)')
set(H2,'LineStyle','--')
grid
axis

% figure
% plot(Time,AREA)
% grid

%close all
Test_plots

```

THIS PAGE INTENTIONALLY LEFT BLANK

## LIST OF REFERENCES

- [Chen, 1993] Chen, C.T., *Analog and Digital Control System Design*, 1<sup>st</sup> Edition, Harcourt Brace Jovanovich Publishers, Orlando, FL, 1993
- [Chernesky, 2001] Chernesky, V.S., "*Development and control of a Three-Axis Satellite Simulator for the Bifocal Relay Mirror Initiative*," M.S. Thesis, Naval Postgraduate School, December 2001
- [Kulick, 2004] Kulick, W J., *Development of a Control Moment Gyroscope Controlled, three Axis Satellite Simulator, with Active Balancing for the Bifocal Relay Mirror Initiative*, M.S. Thesis, Naval Postgraduate School, December 2004
- [Ogata, 2002] Ogata, K, *Modern Control Engineering*. Upper Saddle River, NJ; Prentice Hall, 2002
- [Singh, Singhose] Singh, Tarunraj and Singhose, William, *Tutorial on Input shaping/time delay control of Maneuvering Flexible Structures*
- [Smith, 1957] Smith, O.J.M., "Posicast control of Damped Oscillatory Systems," Proc. Of the IRE, 1957
- [Watkins, 2004] Watkins, J.R., "*The Adaptive Control of Optical Beam Jitter*," PhD Dissertation, December 2004

THIS PAGE INTENTIONALLY LEFT BLANK

## **INITIAL DISTRIBUTION LIST**

1. Defense Technical Information Center  
Ft. Belvoir, Virginia
2. Dudley Knox Library  
Naval Postgraduate School  
Monterey, California
3. Dr. Brij Agrawal  
Naval Postgraduate School  
Monterey, California
4. Dr. Jae Jun Kim  
Naval Postgraduate School  
Monterey, California
5. Michael Doherty  
Naval Postgraduate School  
Monterey, California